Regulation of β1 Integrin-Klf2-mediated angiogenesis by CCM proteins

Marc Renz, Cécile Otten, Eva Faurobert, Franziska Rudolph, Yuan Zhu, Gweńola Boulday, Johan Duchene, Michaela Mickoleit, Ann-Christin Dietrich, Caroline Ramspacher, et al.

Graphical Abstract
Click here to download high resolution image

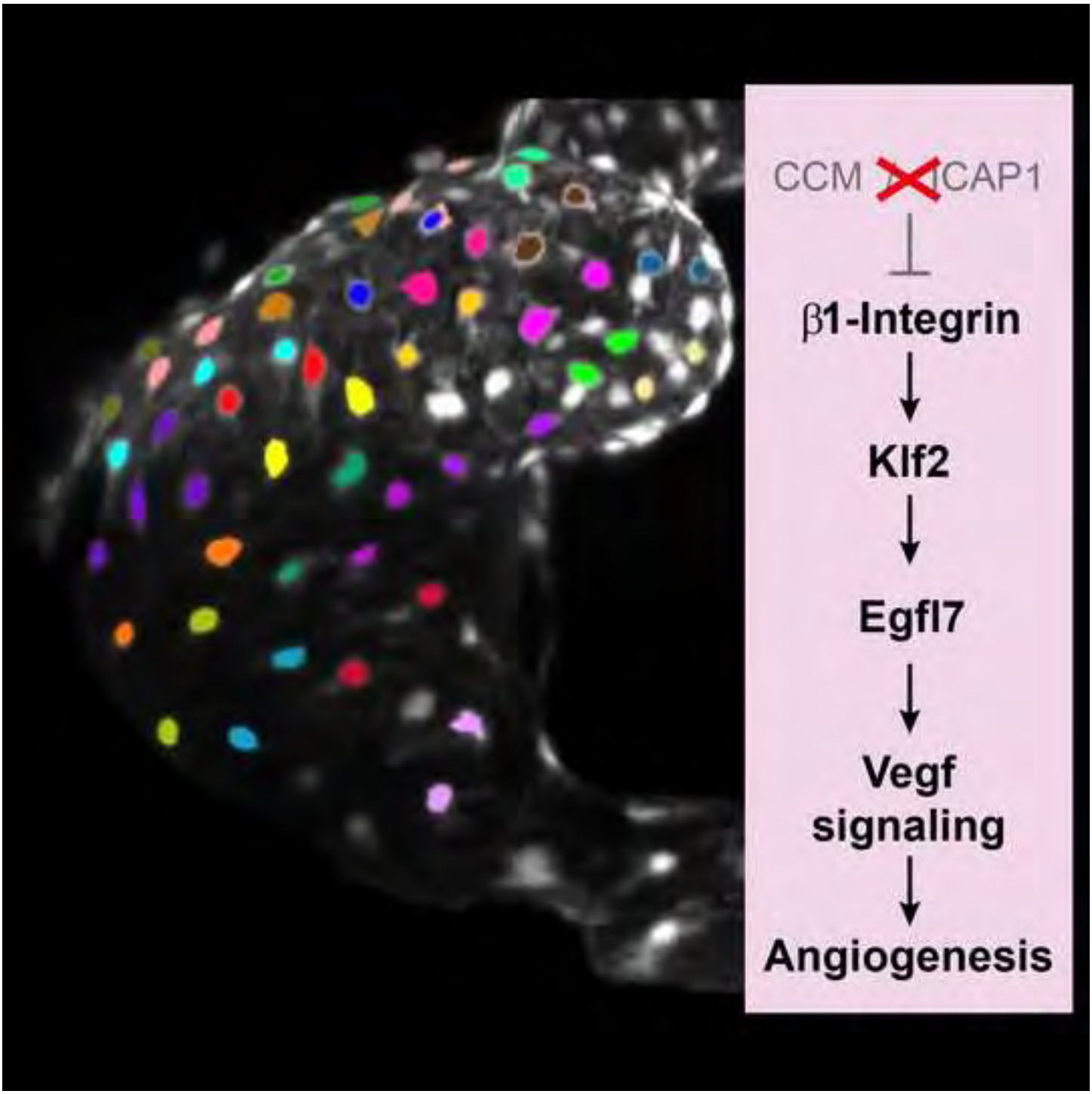

Regulation of β1 Integrin-Klf2-mediated angiogenesis by CCM proteins

Marc Renz[1,2*], Cécile Otten[1,2*], Eva Faurobert[3,4,5], Franziska Rudolph[6], Yuan Zhu[7], Gwénola Boulday[8,9], Johan Duchene[10], Michaela Mickoleit[11], Ann-Christin Dietrich[2], Caroline Ramspacher[12], Emily Steed[12], Sandra Manet-Dupé[3,4,5], Alexander Benz[13], David Hassel[13], Julien Vermot[12], Jan Huisken[11], Elisabeth Tournier-Lasserve[8,9,14], Ute Felbor[15,16], Ulrich Sure[7], Corinne Albiges-Rizo[3,4,5], and Salim Abdelilah-Seyfried[1,2,§]

[1]University Potsdam, Institute for Biochemistry and Biology, Karl-Liebknecht-Strasse. 24-25, House 26, 14476 Potsdam, Germany

[2]Institute for Molecular Biology, Medizinische Hochschule Hannover, 30625 Hannover, Germany

[3]INSERM U823, Institute Albert Bonniot, Grenoble, France

[4]ERL CNRS 5284, Grenoble, France

[5]Université Joseph Fourier, Grenoble, France

[6]Max Delbrück Center for Molecular Medicine Berlin, 13125 Berlin, Germany

[7]Department of Neurosurgery, University of Duisburg-Essen, 45147 Essen, Germany

[8]INSERM, U740, Paris, France

[9]Université Paris Diderot, Sorbonne Paris Cité, Génétique des Maladies vasculaires UMR-S740, Paris, France

[10]Institut für Prophylaxe und Epidemiologie der Kreislaufkrankheiten, Ludwig-Maximilians-Universität München, Pettenkoferstrasse 8a, 80336 München, Germany

[11]Max Planck Institute of Molecular Cell Biology and Genetics, 01307 Dresden, Germany

[12]Institute of Genetics and Molecular and Cellular Biology (IGBMC), CNRS/INSERM/UdS, BP.10142, 67400 Illkirch, France

[13] Universitätsklinikum Heidelberg, Im Neuenheimer Feld 410, 69120 Heidelberg, Germany

[14]AP-HP, Groupe hospitalier Saint-Louis Lariboisière-Fernand-Widal, Service de génétique moléculaire neurovasculaire, Centre de Référence des Maladies Vasculaires Rares du Cerveau et de l'Oeil (CERVCO), Paris, France

[15]Institute of Human Genetics, University Medicine Greifswald, 17475 Greifswald, Germany

[16]Interfaculty Institute for Genetics and Functional Genomics, Division of Human Genetics, Ernst-Moritz-Arndt University Greifswald, Greifswald, Germany

*both authors contributed equally

Running title: Klf2 mechanotransduction in angiogenesis

§Corresponding author: Salim Abdelilah-Seyfried
University Potsdam
Institute for Biochemistry and Biology
Karl-Liebknecht-Strasse. 24-25, House 26
14476 Potsdam
Germany

SUMMARY

Mechanotransduction pathways are activated in response to biophysical stimuli and play important roles in development and the homeostasis of organs and tissues. During zebrafish cardiovascular development, the blood flow-sensitive transcription factor Klf2a promotes VEGF-dependent angiogenesis. However, the role of Klf2a in a mechanotransduction pathway and the means by which such a pathway is regulated to prevent continuous angiogenesis remain unknown. Here we report that the upregulation of *klf2* mRNA causes enhanced *egfl7* expression and angiogenesis signaling, which underlies morphogenetic cardiovascular defects associated with the loss of cerebral cavernous malformations (CCM) proteins in the zebrafish embryo. Using CCM protein-depleted human umbilical vein endothelial cells, we show that the misexpression of *KLF2* mRNA requires the extracellular matrix-binding receptor ß1 integrin and occurs in the absence of blood flow. Downregulation of *ß1 integrin* in zebrafish embryos rescues *ccm* mutant cardiovascular malformations. Our work reveals a novel ß1 integrin-Klf2-Egfl7 signaling pathway that is under tight regulation by CCM proteins and their associated ß1 integrin-regulatory protein ICAP1. This regulation prevents angiogenic overgrowth and ensures the quiescence and correct differentiation of endothelial cells.

INTRODUCTION

During vertebrate embryogenesis, the basic morphology of the cardiovascular system is established prior to the onset of blood flow and is continuously modified in a process referred to as angiogenesis (Herbert and Stainier, 2011; Geudens and Gerhardt, 2011). During angiogenesis, endothelial cells (EC)s respond to biomechanical forces such as hemodynamics or extracellular matrix stiffness (Mammoto et al., 2012; Freund et al., 2012). These biophysical forces can modulate EC quiescence, the stabilization of cellular junctions, blood vessel lumen formation, and the formation of endocardial cushions within the heart. An important mediator of mechanosensitive responses to blood flow within ECs is the zinc-finger transcriptional regulator Krüppel-like factor 2 (KLF2). Within developing zebrafish aortic arch blood vessels, Klf2a activates a signaling cascade involving the endothelial-specific microRNA *miR-126a* that promotes VEGF-induced angiogenesis (Nicoli et al., 2010). Another factor that has been implicated in blood vessel morphogenesis and lumen formation is *EGF-like-domain, multiple 7* (*egfl7*) (Parker et al., 2004), a secreted protein that is associated with the blood vessel extracellular matrix (Soncin et al., 2003; Fitch et al., 2004). That the *egfl7* locus also encodes *mir-126* has complicated functional analyses of different mouse models used to determine the roles of *egfl7* and of *miR-126* in blood vessel development (Schmidt et al., 2007; Kuhnert et al., 2008; Wang et al., 2008). Under physiological conditions, *egfl7* is expressed in the vasculature (Parker et al., 2004) and its promoter contains a putative Klf2 binding site (Harris et al., 2010). Besides a proangiogenic activity, KLF2 also elicits a

broad range of transcriptional changes with a vasoprotective function within ECs of mature blood vessels and promotes the attachment and stability of associated pericytes or vascular smooth muscle cells (Lee et al., 2006; Dekker et al., 2006; Parmar et al., 2006). Within the zebrafish heart, Klf2a is activated by reversible blood flow patterns and is needed for the morphogenesis of functional cardiac valves (Vermot et al., 2009). Despite its pivotal role for vessel remodeling and integrity, neither the precise KLF2 mechanotransduction-related signaling pathway nor the mechanisms involved in the shift from proangiogenic to vasoprotective KLF2 activity are known.

Correct vascular development and integrity involve a complex of proteins called Cerebral Cavernous Malformation (CCM) proteins, which have inhibitory roles during angiogenesis and attenuate Rho kinase signaling which limits vascular permeability (Faurobert and Albiges-Rizo, 2010; Fischer et al., 2013). A loss of any of the three intracellular proteins KRIT1/CCM1, CCM2/OSM, or PDCD10/CCM3 results in cerebral cavernous malformations (Fischer et al., 2013), a group of vascular diseases characterized by cerebral hemorrhages that occur predominantly within low-flow venous capillary beds and that lack typical vessel wall components such as pericytes and vascular smooth muscle cells (Zawistowski et al., 2005; Voss et al., 2007; Zhang et al., 2007). Proteins of the CCM complex assemble around the transmembrane protein Heart of glass (HEG) (Kleaveland et al., 2009). The entire CCM protein complex is involved in endothelial junctional stabilization and directly interacts with the vascular endothelial-Cadherin complex (Glading et al., 2007). In addition, the CCM

complex represses the activity of β1 integrin by stabilizing KRIT1-binding Integrin cytoplasmic domain associated protein 1 (ICAP1) (Faurobert et al., 2013), a specific inhibitor of β1 integrin (Millon-Fremillon et al., 2008) that associates with KRIT1 (Zhang et al., 2001; Zawistowski et al., 2002). β1 integrins are important players in mediating inside-out and outside-in signaling between the intracellular milieu and the extracellular matrix (Hynes, 2002; Ross et al., 2013), and play a role in angiogenesis and vascular development (Avraamides et al., 2008; Carlson et al., 2008; Lei et al., 2008; Tanjore et al., 2008). A paralog of CCM2, CCM2L, has recently been implicated as a promoter of cardiovascular growth by blocking CCM2-mediated vascular integrity (Zheng et al., 2012). Upon loss of PDCD10/CCM3, a separate mechanism involving germinal center kinase III (Chan et al., 2011) or sterile 20-like kinases (Voss et al., 2007; Zheng et al., 2010) has been implicated in defective vascular or *Drosophila* tracheal tube development (Song et al., 2013). Understanding the precise mechanism by which CCM proteins prevent uncontrolled angiogenesis and vessel leakage may provide insights into the mechanisms by which angiogenesis is fine-tuned during vascular maturation and in response to blood flow.

Here, we show that the loss of CCM proteins results in a β1 integrin-dependent overexpression of *klf2*, which in turn causes an upregulation of *egfl7* and promotes angiogenesis. Our findings imply that CCM proteins safeguard endothelial quiescence and restrict proangiogenic signaling in the absence of blood flow-induced biophysical stimuli.

RESULTS

Overexpression of *KLF2* mRNA is a conserved feature of CCM protein-depleted endothelial cells in zebrafish, mouse and HUVECs

A loss of CCM proteins causes a number of cardiovascular malformations in zebrafish and mouse including cardiac ballooning, heart looping defects, a failure of endocardial cushions to form, and defective blood vessel formation (Mably et al., 2003; Mably et al., 2006; Hogan et al., 2008; Boulday et al., 2009; Kleaveland et al., 2009; Zheng et al., 2010; Yoruk et al., 2012). To identify the transcriptional changes responsible for such defects, we performed a comparative transcriptome analysis using cardiac tissue, which is rich in endocardial cells, isolated from *ccm2*^{m201} mutant and wild-type (WT) zebrafish embryos. We found that the two homologous blood-flow-responsive genes *klf2a* and *klf2b* were upregulated in *ccm2*^{m201} mutant hearts; we confirmed the upregulation of *klf2a* and *klf2b* in whole embryos at 48 hours post fertilization (hpf) by RT-qPCR (Fig. 1A). To assess whether the upregulation of *klf2* expression upon loss of CCM proteins is conserved in higher vertebrates, we next analyzed the conditional endothelial deletion of murine *CCM2* (*iCCM2*). The loss of CCM2 within endothelial cells at post-natal day 1 (P1) has been shown to cause cerebral-cavernous-malformations-like vascular defects with a complete penetrance in the cerebellum and in the retina (Boulday et al., 2011). Consistently, we found that *Klf2* mRNA levels were significantly elevated in the cerebellum of such *iCCM2* animals at P15 (Fig. 1B). Strikingly, in *CCM2* siRNA-silenced human umbilical vein endothelial cells (HUVECs), *KLF2* mRNA levels were also increased (Fig.

1C). Hence, *klf2* mRNA overexpression is a conserved feature of CCM protein-depleted ECs.

To further elucidate whether *klf2* overexpression is restricted to particular regions of the zebrafish embryonic vascular network, we next performed whole-mount *in situ* hybridizations. This analysis revealed that *klf2a* and *klf2b* were strongly overexpressed throughout the entire endocardium of zebrafish *krit1*^{ty219c} and *ccm2*^{m201} mutants (Fig. 1D-F; supplementary Fig. S1) and within arteries and veins of *ccm2*^{m201} mutants (Fig. 1G,H). Taken together, these findings show that a loss of CCM proteins causes an upregulation of *klf2* mRNA within different regions of the vascular network.

Elevated levels of *klf2* are necessary and sufficient to induce cardiovascular malformation phenotypes associated with the loss of CCM proteins in zebrafish

Klf2 proteins are blood-flow responsive endothelial transcription factors with essential roles in vasculogenesis, angiogenesis, cardiac valve morphogenesis, regulation of vascular tone, and control of vasoprotective gene expression (Dekker et al., 2006; Lee et al., 2006; Parmar et al., 2006; Vermot et al., 2009; Nicoli et al., 2010). Based on the different cardiovascular functions of Klf2, we assessed whether high expression levels of *klf2a* and *klf2b* may be causative for the *ccm2*^{m201} mutant cardiovascular phenotype. The *ccm2*^{m201} cardiac phenotype is characterized by cardiac ballooning, endocardial overproliferation, and by a lack of cardiac cushions that normally form by 48hpf, as evidenced by the failure of endocardial cells to acquire a cuboidal shape and to express activated

leukocyte cell adhesion molecule (Alcam) (Fig. 2A-B',J) (Jin et al., 2005). Within the *ccm2*^{m201} mutant vasculature, the lateral dorsal aortae (LDA) exhibit significant increases in endothelial cell numbers at 48 hpf, providing evidence for increased angiogenesis signaling (Fig. 2D,E,J). Similarly, within the trunk region region of *ccm2*^{m201} mutants, the subintestinal vein (SIV) exhibits a higher density of vessel branch points, which is another established marker for increased angiogenesis (Yu et al., 2010; Avraham-Davidi et al., 2012; Ghajar et al., 2013) (Fig. 2G,H,K).

Strikingly, the partial reduction of both Klf2 proteins by coinjection of low doses of two antisense oligonucleotide morpholinos (MOs) (5ng each) completely restored endocardial cushion formation, cardiac chamber morphogenesis, and even restored some blood flow within the heart and major blood vessels in *ccm2*^{m201}, *krit1*^{ty219c}, and *heg*^{m552} mutants (complete rescue was observed for at least n>50 embryos of each genotype verified by genotyping; high-resolution confocal images were recorded for n=5 mutant embryos with invariant results) (Fig. 2C,C'; supplementary Fig. S2). That low doses of both MOs were sufficient for the rescue of cardiac morphology suggests that Klf2 protein levels are down-regulated towards normal expression levels by this injection regiment. In comparison, the injection of high doses of MOs against either *klf2a* or *klf2b* (12ng each) did not rescue the cardiac phenotype of *ccm2*^{m201} mutants, which shows that both Klf2 proteins are involved in the *ccm* mutant phenotype (Supplementary Fig. S2A-H'). Consistent with the previous results, the low-dose knock-down of *klf2a* and *klf2b* in *ccm2*^{m201} mutants rescued endocardial and LDA cell numbers

(Fig. 2F,J) and reduced the number of SIV branch points (Fig. 2I,K). Our results indicated that the two *klf2* genes play a central role in mediating the different cardiovascular malformations associated with the loss of CCM proteins.

To directly examine whether the induction of *klf2a* in WT embryos was also sufficient to phenocopy *ccm2*^{m201} mutant cardiovascular defects, we used stable transgenic lines for overexpression of *klf2a* from a *friend leukemia integration 1a* (*fli1a*) promoter [Tg(*fli1ep:GAL4FF*)^{ubs2} (Herwig et al., 2011) and Tg(*UAS:klf2a*)$^{ig1-3}$]. The continuous endothelial-specific overexpression of *klf2a* in these lines begins at endocardial progenitor stages, prior to heart formation, and causes a cardiac ballooning phenotype between 48-72 hpf with a high penetrance of ~80% (n= 36/43 transgenic embryos out of 3 independent F1 transgenic lines), comparable to the *ccm2*^{m201}mutant cardiac phenotype (Fig. 2L,M). Similarly, ubiquitous overexpression of *klf2a* from a heat-shock promoter induced at 15, 30, and again at 38 hpf [Tg(*hsp70l:klf2a*)^{md8}], resulted in increased LDA cell numbers at 48 hpf, comparable to those in *ccm2*^{m201} mutants (Fig. 2J). Taken together, the overexpression of *klf2a*/*b* in zebrafish is necessary and sufficient for the expression of cardiovascular malformation phenotypes associated with the loss of CCM proteins.

Klf2 promotes proangiogenic signaling and increases the expression of Egfl7

Several lines of evidence suggest that aberrant angiogenesis may be associated with the loss of CCM proteins: Human cerebral cavernous malformations lesion

growth is correlated with increased circulating concentrations of VEGF (Jung et al., 2003), mice heterozygous for a mutation in *CCM2* have increased vascular permeability in response to injection of VEGF (Whitehead et al., 2009), and angiogenesis signaling is increased in endothelial cells lacking CCM proteins (Wustehube et al., 2010; Zhu et al., 2010). In addition, the misregulation of angiogenic VEGF signaling has an inhibitory effect on cardiac cushion formation in mice (Dor et al., 2001). In agreement with these observations, we found that several genes related to angiogenesis signaling were upregulated in *ccm2*^{m201} mutant compared with WT zebrafish cardiac transcriptomes (Table 1).

To determine whether *ccm2*^{m201} mutant cardiovascular defects are due to aberrant angiogenesis, we inhibited VEGF signaling in *ccm2*^{m201} mutants using the pharmacological compound PTK787 (Chan et al., 2002). Under this anti-angiogenic condition, we observed a rescue of *ccm* mutant cardiovascular defects, including cardiac cushion defects (Fig. 3A-C') and overproliferation defects of endocardium and LDA (Fig. 3D). Based on this evidence, we also assayed whether the PTK787 inhibition of angiogenesis would affect *klf2a*/*b* mRNA levels in *ccm2*^{m201} mutants, which is not the case (Fig. 3E). Hence, *klf2a*/*b* mRNA expression is misregulated independently of VEGFR-mediated angiogenesis in *ccm2*^{m201} mutants. Taken together, our results indicate that Klf2 proteins promote proangiogenic signaling.

Of particular interest among the angiogenesis-related genes that were upregulated upon loss of zebrafish Ccm2, was the *EGF-like-domain, multiple 7* (*egfl7*) gene (Parker et al., 2004), which contains a putative Klf2 binding site

(Harris et al., 2010). We verified the increased expression levels of *egfl7* in *ccm2*^{m201} mutants by comparative RT-qPCR (Fig. 4A). To assess whether the overexpression of *klf2* was sufficient to induce higher levels of *egfl7* expression, we induced *klf2a/b* in Tg(*hsp70l:klf2a_IRES_EGFP*)^{md8} or Tg(*hsp70l:klf2b_IRES_EGFP*)^{md9} transgenic embryos and found that, consistent with a regulation by *klf2* genes, the expression levels of *egfl7* mRNA were enhanced under this condition (Fig. 4A). Similarly, in HUVECs, levels of *EGFL7* were elevated upon silencing of ICAP1, KRIT1 or CCM2 (Fig. 4B).

These findings suggested that *egfl7* is regulated downstream of Klf2, which prompted us to further elucidate its potential involvement in *ccm2*^{m201} mutant cardiovascular malformations. Strikingly, *ccm2*^{m201} mutant cardiovascular defects, including the lack of cardiac cushions were rescued upon using a low dose of an *egfl7*MO (0.6ng) (Fig. 4C-E'). Hence, similar to Klf2 proteins, high levels of Egfl7 mediate cardiovascular defects associated with the loss of CCM proteins. To more directly test whether *klf2a/b* and *egfl7* interact genetically, we co-injected *klf2a/b* (2.5 ng each) and *egfl7* MOs (0.3 ng) at low doses that individually did not rescue the *ccm2*^{m201} mutant cardiovascular phenotypes including lumenization defects within intersegmental vessels that arise due to a lack of cardiac function (no rescue among n>50 *ccm2*^{m201} mutants tested for each MO; supplementary Fig. S3D,E). The triple MO injection rescued the cardiovascular defects in *ccm2*^{m201} mutant embryos as indicated by the lumenization of intersegmental vessels (n=19/21 *ccm2*^{m201} mutants rescued,

verified by genotyping; supplementary Fig. S3C) and further solidified our finding that *klf2a/b* and *egfl7* act in a common pathway.

Contrary to the misregulation of *egfl7*, neither *miR-126a* (which is required for aortic arch formation in zebrafish) nor *miR-126b* (which is located within the *egfl7* gene) were misregulated in *ccm2*^{m201} mutants based on RT-qPCR experiments on 48 hpf whole embryos (Supplementary Fig. S4). Taken together, our results indicate that Klf2 proteins promote VEGF-dependent proangiogenic signaling, possibly by increasing the expression of Egfl7.

Overexpression of *klf2* within CCM-ICAP1-depleted endothelium involves β1 integrin but is independent of blood flow

Within the zebrafish heart, Klf2a is activated in response to reversible blood flow (Vermot et al., 2009). This finding raised the question of whether another biophysical force-related mechanism might be involved in the induction of *klf2a*/*b* in *ccm* mutants, since they have only severely reduced blood flow. To determine whether *klf2a*/*b* expression is indeed flow-independent in *ccm* mutants, we used a MO to knock down *troponin t2a* (*tnnt2a*). The absence of Tnnt2a causes a loss of cardiac contractility due to myofibrillar defects and a complete lack of blood flow, which zebrafish embryos survive for several days (Sehnert et al., 2002). We found that under such no-flow conditions, *ccm2*^{m201} mutant cardiac phenotypes (Fig. 5A-C) and elevated *klf2a* and *klf2b* mRNA levels were not rescued (Fig. 5D). Hence, expression levels of *klf2a*/*b* mRNA and the occurrence of cardiovascular malformations in *ccm2*^{m201} mutants are truly independent of the mechanical stimulation of ECs by blood flow. Time-lapse analyses between 33-

53 hpf of *ccm2*^{m201} mutant; *tnnt2a* morphants using light-sheet illumination microscopy (SPIM) showed that the Ccm2-deficient endocardium is highly proliferative in absence of blood flow, contrary to *tnnt2a* morphants (Fig. 5E-G; supplementary movies 1,2). Similarly, human cerebral cavernoma form in venous capillary beds that are characterized by low-blood-flow conditions (Supplementary movie 3). Therefore, another stimulus rather than shear stress must be involved in the activation of the KLF2 mechanotransduction pathway in CCM protein-depleted ECs.

In HUVECs, ICAP1 directly interacts with and attenuates the activity of β1 integrin (Millon-Fremillon et al., 2008; Faurobert et al., 2013). Depletion of KRIT1 causes the destabilization of ICAP1 protein resulting in increased β1 integrin activation (Faurobert et al., 2013). In addition, knock-out of *ICAP1* in mouse leads to vascular defects such as excessive branching and dilation (Faurobert et al., 2013). To elucidate the potential involvement of β1 integrin in KLF2-dependent mechanotransduction, we first used HUVECs to assess *KLF2* mRNA expression upon simultaneously silencing *β1 integrin* and either *KRIT1*, *CCM2* or *ICAP1*. We found that β1 integrin was required for high expression levels of *KLF2* mRNA in CCM protein-depleted HUVECs (Fig. 6A; efficacy of siRNA knockdowns is shown in supplemental Fig. S5). In a complementary set of experiments, we used a MO to downregulate *β1b integrin* in zebrafish *ccm2*^{m201} mutants (Ablooglu et al., 2010). Remarkably, low doses of β1b integrin MO rescued cardiovascular malformations including the loss of cardiac cushions (n=5/5 *ccm2*^{m201} mutant embryos rescued; Fig. 6B-D'). Taken together, these

findings showed that β1 integrin contributes to *KLF2* mRNA expression and promotes angiogenesis by enhancing Klf2 proangiogenic signaling. These findings imply that CCM proteins attenuate angiogenesis signaling during blood vessel maturation by negatively modulating the activity of integrins.

DISCUSSION

Our study demonstrates that the shear stress-sensitive transcription factor Klf2 is a major player in CCM-dependent vascular development in zebrafish. We found that Klf2 is strongly overexpressed independently of blood flow when CCM proteins are lost and that β1 integrin is a signal triggering this elevated *klf2* expression. Finally, we suggest that the proangiogenic activity of Klf2 is based on the stimulation of Egfl7. These findings identify the CCM complex as a key regulator of a novel β1 integrin-Klf2-Egfl7 mechanotransduction pathway in zebrafish. This regulation prevents angiogenic overgrowth and ensures the quiescence and differentiation of endothelial and endocardial cells. One implication of our findings is that extracellular matrix mechanics mediated by β1 integrin signaling and cellular tension generated within endothelial cells is sufficient to activate the mechanosensitive transcription factor Klf2 even in a blood-flow-independent manner. The misregulation of cellular tension in *ccm* mutants may cause the developmental defects described in our study.

Given the current controversy on the functional role of Egfl7 in blood vessel development, our work now provides further evidence that expression levels of Egfl7 are an important factor in blood vessel development. Initial functional studies suggested that loss of *egfl7* in mice and zebrafish causes vascular defects (Parker et al., 2004; Schmidt et al., 2007). However, in mouse, these phenotypes were later attributed to the inactivation of *miR-126* within the *egfl7* locus (Kuhnert et al., 2008; Wang et al., 2008). We show here that elevated levels of *egfl7* in *ccm2*^{m201} mutants correlate with abnormal angiogenesis and

that down-regulating the expression levels of *egfl7* rescues the mutant cardiac phenotype. This finding is in tune with a report that overexpression of *egfl7* specifically in endothelial cells induces cardiac and blood vessel defects in mice (Nichol et al., 2010). In comparison, *miR-126a* or *miR-126b* were not misregulated in *ccm2*^{m201} mutants. We conclude that the elevated expression levels of *klf2* and *egfl7* mediate the *ccm* phenotype independently of *miR-126*.

Previous studies have not explained why mature, post-angiogenic, and well perfused blood vessels are largely resistant to the loss of CCM proteins in mice. Instead, the loss of CCM proteins mainly affects low-blood-flow venous capillary beds. Our study indicates that KLF2 could be a player in this pathology since it controls EC gene expression in response to blood flow with biphasic roles depending on the biological context. Within regions of high laminar shear stress, the induction of KLF2 establishes vasoprotective gene expression within vessel walls (Dekker et al., 2006; Parmar et al., 2006), explaining why high shear-stress regions of the human vasculature are mostly protected from cerebral cavernous malformation-like lesions. In contrast, lowly-perfused small venous capillary beds may be more prone to vascular malformations due to the proangiogenic role of KLF2 (Nicoli et al., 2010), which is enhanced by β1 integrin. In support of this model, data obtained in constitutive *iCCM2* knockout embryonic mice reveal strong developmental phenotypes within the cardiovascular system under impaired low-flow conditions. Mice targeted post-natally, in which high-flow conditions within the heart and arteries have been established, show only capillarovenous disease-like phenotypes (Boulday et al., 2011). In principle, low

blood flow and hypoxic conditions or proangiogenic stimuli from neighboring tissues may enhance a proangiogenic KLF2 response that perpetuates the formation of cerebral cavernous malformation lesions. A number of studies have suggested that hypoxic conditions in older patients (Denier et al., 2006; Labauge et al., 2007) or signaling from neural tissue may trigger the development of cerebral cavernous malformation lesions within neighboring venous capillaries (Louvi et al., 2011).

Our work introduces the idea that the CCM complex has an essential role in limiting β1 integrin-mediated expression of *KLF2* in ECs, thereby attenuating VEGF-dependent angiogenesis signaling (Fig. 6E). Future research should reveal whether this pathway is relevant for other vascular pathologies as well. For instance, genetic and molecular evidence from inheritable forms of aneurysms points to an involvement of aberrant TGF-β signaling in these vascular diseases (Pardali et al., 2010; Lindsay and Dietz, 2011). Intriguingly, murine *KLF2* knockout animals frequently present with aortic aneuryms (Kuo et al., 1997). Aberrant TGF-β (Pardali et al., 2010; Lindsay and Dietz, 2011; Maddaluno et al., 2013) or angiogenesis (Wustehube et al., 2010) signaling is found in a plethora of vascular diseases including cerebral cavernous malformations. Our work now opens an intriguing possibility that inappropriate changes in *KLF2* may lie at the heart of many other pathologies of the human vasculature both under conditions of low-blood-flow (leading to an enhanced proangiogenic KLF2 activity) and also under high-blood-flow (where there is a loss of vasoprotective KLF2 activity).

EXPERIMENTAL PROCEDURES

Zebrafish lines and handling. Handling of zebrafish was done in compliance with German and Berlin state law, carefully monitored by the local authority for animal protection (LaGeSo, Berlin-Brandenburg, Germany). The following strains were maintained under standard conditions as previously described (Westerfield et al., 1997): *ccm2*^{m201} (Mably et al., 2006), *krit1*^{ty219c} (Mably et al., 2006), *heg*^{m552} (Mably et al., 2003), Tg(*myl7:GFP*)^{twu34} (Huang et al., 2003), Tg(*kdrl:GFP*)^{s843} (Jin et al., 2005), Tg(*fli1a:GAL4FF*)^{ubs2} (Herwig et al., 2011), Tg(*UAS:KLF2a*)$^{ig1-3}$, Tg(*hsp70l:klf2a_IRES_EGFP*)^{md8}, Tg(*hsp70l:klf2b_IRES_EGFP*)$^{md9-11}$. The following morpholinos were used: *klf2a* (GGACCTGTCCAGTTCATCCTTCCAC) (Nicoli et al., 2010), *klf2b* (AAAGGCAAGGTAAAGCCATGTCCAC), *tnnt2a* (CATGTTTGCTCTGATCTGACACGCA) (Sehnert et al., 2002), *itgb1b* (GCCAGTTTGAGTGAATAACTCACCT) (Ablooglu et al., 2010).
See Supplemental Information for details on morpholino injections, heat-shock and pharmacological treatment conditions, and on the generation of transgenic lines.

Immunohistochemistry. For zebrafish whole-mount immunohistochemistry, the following antibodies were used: mouse Zn-8/Alcam (1:100; Developmental Studies Hybridoma Bank); Cy5-conjugated secondary antibody goat-anti-mouse (1:250; Jackson ImmunoResearch Laboratories cat# 96829); Rhodamine Phalloidine was used to stain Actin (1:100; Sigma cat# 658740). For details, also on quantifications of endocardial and LDA cell numbers, see Supplemental Information.

Whole-mount *in situ* hybridizations. Zebrafish embryos were collected at 48hpf, fixed with 4% paraformaldehyde overnight at 4°C and *in situ* hybridization with *klf2a* and *klf2b in situ* probes was performed as described elsewhere (Jowett and Lettice, 1994). For details, see Supplemental Information.

Quantitative RT-qPCR. To determine *klf2* expression levels, RT-qPCR experiments were performed on zebrafish whole embryos, on *iCCM2* mouse cerebella (Boulday, 2009), and on HUVECs in compliance with the MIQE standard (Bustin et al., 2009). See Supplemental Informations for details on samples, conditions and primers used for RT-qPCR, and data analysis.

Selective plane illumination microscopy (SPIM) imaging. SPIM imaging was performed with zebrafish *tnnt2a* morphants and *ccm2*^{m201}; *tnnt2a* mutant/morphant embryos harboring the Tg(*kdrl:GFP*)^{s843} transgene between 33 and 53 hpf. See Supplemental Informations for details on samples and analysis of the recordings.

Video angiography during neurosurgical procedures. Video angiography of a human cavernoma was performed during a neurosurgical procedure as previously described (Raabe et al., 2003). See Supplemental Informations for further details.

AUTHOR CONTRIBUTIONS

M. R., C. O., E. F., C. A.-R., and S.A.-S. contributed to the conception and design of the experiments. Y.Z., C.R., E.S., S.M.-D., J.V., J.H., D.H., A.B., U.F., and U.S. contributed reagents, transgenic animals or tissue, data, and movies.

They also helped with the interpretation of this data and discussions on the project. M. R., C. O., E. F., F. R., J. D., A.B., M.M., and A.-C.D. collected the data. M. R., C. O., E. F., C. A.-R., D.H., G.B., E.T.-L., and S.A.-S. interpreted and analyzed the data. C.O., M.R. and S. A.-S. wrote the manuscript.

REFERENCES

Ablooglu,A.J., Tkachenko,E., Kang,J., and Shattil,S.J. (2010). Integrin alphaV is necessary for gastrulation movements that regulate vertebrate body asymmetry. Development *137*, 3449-3458.

Avraham-Davidi,I., Ely,Y., Pham,V.N., Castranova,D., Grunspan,M., Malkinson,G., Gibbs-Bar,L., Mayseless,O., Allmog,G., Lo,B., Warren,C.M., Chen,T.T., Ungos,J., Kidd,K., Shaw,K., Rogachev,I., Wan,W., Murphy,P.M., Farber,S.A., Carmel,L., Shelness,G.S., Iruela-Arispe,M.L., Weinstein,B.M., and Yaniv,K. (2012). ApoB-containing lipoproteins regulate angiogenesis by modulating expression of VEGF receptor 1. Nat. Med. *18*, 967-973.

Avraamides, C.J., Garmy-Susini, B., and Varner, J.A.(2008). Integrins in angiogenesis and lymphangiogenesis. Nat. Rev. Cancer.*8*, 604-17.

Beis,D., Bartman,T., Jin,S.W., Scott,I.C., D'Amico,L.A., Ober,E.A., Verkade,H., Frantsve,J., Field,H.A., Wehman,A., Baier,H., Tallafuss,A., Bally-Cuif,L., Chen,J.N., Stainier,D.Y., and Jungblut,B. (2005). Genetic and cellular analyses of zebrafish atrioventricular cushion and valve development. Development *132*, 4193-4204.

Boulday,G., Blecon,A., Petit,N., Chareyre,F., Garcia,L.A., Niwa-Kawakita,M., Giovannini,M., and Tournier-Lasserve,E. (2009). Tissue-specific conditional CCM2 knockout mice establish the essential role of endothelial CCM2 in angiogenesis: implications for human cerebral cavernous malformations. Dis. Model. Mech. *2*, 168-177.

Boulday,G., Rudini,N., Maddaluno,L., Blecon,A., Arnould,M., Gaudric,A., Chapon,F., Adams,R.H., Dejana,E., and Tournier-Lasserve,E. (2011). Developmental timing of CCM2 loss influences cerebral cavernous malformations in mice. J. Exp. Med. *208*, 1835-1847.

Bustin,S.A., Benes,V., Garson,J.A., Hellemans,J., Huggett,J., Kubista,M., Mueller,R., Nolan,T., Pfaffl,M.W., Shipley,G.L., Vandesompele,J., and Wittwer,C.T. (2009). The MIQE guidelines: minimum information for publication of quantitative real-time PCR experiments. Clin. Chem. *55*, 611-622.

Carlson, T.R., Hu, H., Braren, R., Kim, Y.H., and Wang, R.A. (2008). Cell-autonomous requirement for beta1 integrin in endothelial cell adhesion, migration and survival during angiogenesis in mice. Development *135*, 2193-202.

Chan,A.C., Drakos,S.G., Ruiz,O.E., Smith,A.C., Gibson,C.C., Ling,J., Passi,S.F., Stratman,A.N., Sacharidou,A., Revelo,M.P., Grossmann,A.H., Diakos,N.A., Davis,G.E., Metzstein,M.M., Whitehead,K.J., and Li,D.Y. (2011). Mutations in 2 distinct genetic pathways result in cerebral cavernous malformations in mice. J. Clin. Invest *121*, 1871-1881.

Chan,J., Bayliss,P.E., Wood,J.M., and Roberts,T.M. (2002). Dissection of angiogenic signaling in zebrafish using a chemical genetic approach. Cancer Cell *1*, 257-267.

Dekker,R.J., Boon,R.A., Rondaij,M.G., Kragt,A., Volger,O.L., Elderkamp,Y.W., Meijers,J.C., Voorberg,J., Pannekoek,H., and Horrevoets,A.J. (2006). KLF2 provokes a gene expression pattern that establishes functional quiescent differentiation of the endothelium. Blood *107*, 4354-4363.

Denier,C., Labauge,P., Bergametti,F., Marchelli,F., Riant,F., Arnoult,M., Maciazek,J., Vicaut,E., Brunereau,L., and Tournier-Lasserve,E. (2006). Genotype-phenotype correlations in cerebral cavernous malformations patients. Ann. Neurol. *60*, 550-556.

Dor,Y., Camenisch,T.D., Itin,A., Fishman,G.I., McDonald,J.A., Carmeliet,P., and Keshet,E. (2001). A novel role for VEGF in endocardial cushion formation and its potential contribution to congenital heart defects. Development *128*, 1531-1538.

Faurobert,E. and Albiges-Rizo,C. (2010). Recent insights into cerebral cavernous malformations: a complex jigsaw puzzle under construction. FEBS J. *277*, 1084-1096.

Faurobert,E., Rome,C., Lisowska,J., Manet-Dupe,S., Boulday,G., Malbouyres,M., Balland,M., Bouin,A.P., Keramidas,M., Bouvard,D., Coll,J.L., Ruggiero,F., Tournier-Lasserve,E., and Albiges-Rizo,C. (2013). CCM1-ICAP-1 complex controls beta1 integrin-dependent endothelial contractility and fibronectin remodeling. J. Cell Biol. *202*, 545-561.

Fischer,A., Zalvide,J., Faurobert,E., Albiges-Rizo,C., and Tournier-Lasserve,E. (2013). Cerebral cavernous malformations: from CCM genes to endothelial cell homeostasis. Trends Mol. Med. *19*, 302-308.

Fitch, M.J., Campagnolo, L., Kuhnert, F., and Stuhlmann, H. (2004). Egfl7, a novel epidermal growth factor-domain gene expressed in endothelial cells. *Dev. Dyn. 230*, 316–24.

Freund,J.B., Goetz,J.G., Hill,K.L., and Vermot,J. (2012). Fluid flows and forces in development: functions, features and biophysical principles. Development *139*, 1229-1245.

Geudens,I. and Gerhardt,H. (2011). Coordinating cell behaviour during blood vessel formation. Development *138*, 4569-4583.

Ghajar,C.M., Peinado,H., Mori,H., Matei,I.R., Evason,K.J., Brazier,H., Almeida,D., Koller,A., Hajjar,K.A., Stainier,D.Y., Chen,E.I., Lyden,D., and Bissell,M.J. (2013). The perivascular niche regulates breast tumour dormancy. Nat. Cell Biol. *15*, 807-817.

Glading,A., Han,J., Stockton,R.A., and Ginsberg,M.H. (2007). KRIT-1/CCM1 is a Rap1 effector that regulates endothelial cell cell junctions. J. Cell Biol. *179*, 247-254.

Harris,T.A., Yamakuchi,M., Kondo,M., Oettgen,P., and Lowenstein,C.J. (2010). Ets-1 and Ets-2 regulate the expression of microRNA-126 in endothelial cells. Arterioscler. Thromb. Vasc. Biol. *30*, 1990-1997.

Herbert,S.P. and Stainier,D.Y. (2011). Molecular control of endothelial cell behaviour during blood vessel morphogenesis. Nat. Rev. Mol. Cell Biol. *12*, 551-564.

Herwig,L., Blum,Y., Krudewig,A., Ellertsdottir,E., Lenard,A., Belting,H.G., and Affolter,M. (2011). Distinct cellular mechanisms of blood vessel fusion in the zebrafish embryo. Curr. Biol. *21*, 1942-1948.

Hogan,B.M., Bussmann,J., Wolburg,H., and Schulte-Merker,S. (2008). ccm1 cell autonomously regulates endothelial cellular morphogenesis and vascular tubulogenesis in zebrafish. Hum. Mol. Genet. *17*, 2424-2432.

Huang,C.J., Tu,C.T., Hsiao,C.D., Hsieh,F.J., and Tsai,H.J. (2003). Germ-line transmission of a myocardium-specific GFP transgene reveals critical regulatory elements in the cardiac myosin light chain 2 promoter of zebrafish. Dev. Dyn. *228*, 30-40.

Huisken,J. and Stainier,D.Y. (2009). Selective plane illumination microscopy techniques in developmental biology. Development *136*, 1963-1975.

Hynes,R.O. (2002). Integrins: bidirectional, allosteric signaling machines. Cell *110*, 673-687.

Jin,S.W., Beis,D., Mitchell,T., Chen,J.N., and Stainier,D.Y. (2005). Cellular and molecular analyses of vascular tube and lumen formation in zebrafish. Development *132*, 5199-5209.

Jowett,T. and Lettice,L. (1994). Whole-mount in situ hybridizations on zebrafish embryos using a mixture of digoxigenin- and fluorescein-labelled probes. Trends Genet. *10*, 73-74.

Jung,K.H., Chu,K., Jeong,S.W., Park,H.K., Bae,H.J., and Yoon,B.W. (2003). Cerebral cavernous malformations with dynamic and progressive course: correlation study with vascular endothelial growth factor. Arch. Neurol. *60*, 1613-1618.

Kaufmann,A., Mickoleit,M., Weber,M., and Huisken,J. (2012). Multilayer mounting enables long-term imaging of zebrafish development in a light sheet microscope. Development *139*, 3242-3247.

Kleaveland,B., Zheng,X., Liu,J.J., Blum,Y., Tung,J.J., Zou,Z., Sweeney,S.M., Chen,M., Guo,L., Lu,M.M., Zhou,D., Kitajewski,J., Affolter,M., Ginsberg,M.H., and Kahn,M.L. (2009). Regulation of cardiovascular development and integrity by the heart of glass-cerebral cavernous malformation protein pathway. Nat. Med. *15*, 169-176.

Kuhnert, F., Mancuso, M.R., Hampton, J., Stankunas, K., Asano, T., Chen, C.Z., Kuo, C.J. (2008). Attribution of vascular phenotypes of the murine Egfl7 locus to the microRNA *miR-126*. Development *135*, 3989-93.

Kuo,C.T., Veselits,M.L., Barton,K.P., Lu,M.M., Clendenin,C., and Leiden,J.M. (1997). The LKLF transcription factor is required for normal tunica media formation and blood vessel stabilization during murine embryogenesis. Genes Dev. *11*, 2996-3006.

Kwan,K.M., Fujimoto,E., Grabher,C., Mangum,B.D., Hardy,M.E., Campbell,D.S., Parant,J.M., Yost,H.J., Kanki,J.P., and Chien,C.B. (2007). The Tol2kit: a multisite gateway-based construction kit for Tol2 transposon transgenesis constructs. Dev. Dyn. *236*, 3088-3099.

Labauge,P., Denier,C., Bergametti,F., and Tournier-Lasserve,E. (2007). Genetics of cavernous angiomas. Lancet Neurol. *6*, 237-244.

Lee,J.S., Yu,Q., Shin,J.T., Sebzda,E., Bertozzi,C., Chen,M., Mericko,P., Stadtfeld,M., Zhou,D., Cheng,L., Graf,T., Macrae,C.A., Lepore,J.J., Lo,C.W., and Kahn,M.L. (2006). Klf2 is an essential regulator of vascular hemodynamic forces in vivo. Dev. Cell *11*, 845-857.

Lei, L., Liu, D., Huang, Y., Jovin, I., Shai, S.Y., Kyriakides, T., Ross, R.S., and Giordano, F.J.. (2008). Endothelial expression of beta1 integrin is required for embryonic vascular patterning and postnatal vascular remodeling. Mol Cell Biol. *28*, 794-802.

Lindsay,M.E. and Dietz,H.C. (2011). Lessons on the pathogenesis of aneurysm from heritable conditions. Nature *473*, 308-316.

Louvi,A., Chen,L., Two,A.M., Zhang,H., Min,W., and Gunel,M. (2011). Loss of cerebral cavernous malformation 3 (Ccm3) in neuroglia leads to CCM and vascular pathology. Proc. Natl. Acad. Sci. U. S. A *108*, 3737-3742.

Mably,J.D., Chuang,L.P., Serluca,F.C., Mohideen,M.A., Chen,J.N., and Fishman,M.C. (2006). santa and valentine pattern concentric growth of cardiac myocardium in the zebrafish. Development *133*, 3139-3146.

Mably,J.D., Mohideen,M.A., Burns,C.G., Chen,J.N., and Fishman,M.C. (2003). heart of glass regulates the concentric growth of the heart in zebrafish. Curr. Biol. *13*, 2138-2147.

Maddaluno,L., Rudini,N., Cuttano,R., Bravi,L., Giampietro,C., Corada,M., Ferrarini,L., Orsenigo,F., Papa,E., Boulday,G., Tournier-Lasserve,E., Chapon,F., Richichi,C., Retta,S.F., Lampugnani,M.G., and Dejana,E. (2013). EndMT contributes to the onset and progression of cerebral cavernous malformations. Nature *498*, 492-496.

Mammoto,A., Mammoto,T., and Ingber,D.E. (2012). Mechanosensitive mechanisms in transcriptional regulation. J. Cell Sci. *125*, 3061-3073.

Millon-Fremillon,A., Bouvard,D., Grichine,A., Manet-Dupe,S., Block,M.R., and Albiges-Rizo,C. (2008). Cell adaptive response to extracellular matrix density is controlled by ICAP-1-dependent beta1-integrin affinity. J. Cell Biol. *180*, 427-441.

Nichol,D., Shawber,C., Fitch,M.J., Bambino,K., Sharma,A., Kitajewski,J., and Stuhlmann,H. (2010). Impaired angiogenesis and altered Notch signaling in mice overexpressing endothelial Egfl7. Blood *116*, 6133-6143.

Nicoli,S., Standley,C., Walker,P., Hurlstone,A., Fogarty,K.E., and Lawson,N.D. (2010). MicroRNA-mediated integration of haemodynamics and Vegf signalling during angiogenesis. Nature *464*, 1196-1200.

Pardali,E., Goumans,M.J., and ten,D.P. (2010). Signaling by members of the TGF-beta family in vascular morphogenesis and disease. Trends Cell Biol. *20*, 556-567.

Parker,L.H., Schmidt,M., Jin,S.W., Gray,A.M., Beis,D., Pham,T., Frantz,G., Palmieri,S., Hillan,K., Stainier,D.Y., De Sauvage,F.J., and Ye,W. (2004). The endothelial-cell-derived secreted factor Egfl7 regulates vascular tube formation. Nature *428*, 754-758.

Parmar,K.M., Larman,H.B., Dai,G., Zhang,Y., Wang,E.T., Moorthy,S.N., Kratz,J.R., Lin,Z., Jain,M.K., Gimbrone,M.A., Jr., and Garcia-Cardena,G. (2006). Integration of flow-dependent endothelial phenotypes by Kruppel-like factor 2. J. Clin. Invest *116*, 49-58.

Raabe,A., Beck,J., Gerlach,R., Zimmermann,M., and Seifert,V. (2003). Near-infrared indocyanine green video angiography: a new method for intraoperative assessment of vascular flow. Neurosurgery *52*, 132-139.

Ross,T.D., Coon,B.G., Yun,S., Baeyens,N., Tanaka,K., Ouyang,M., and Schwartz,M.A. (2013). Integrins in mechanotransduction. Curr. Opin. Cell Biol. *25*, 613-618.

Schindelin,J., Arganda-Carreras,I., Frise,E., Kaynig,V., Longair,M., Pietzsch,T., Preibisch,S., Rueden,C., Saalfeld,S., Schmid,B., Tinevez,J.Y., White,D.J., Hartenstein,V., Eliceiri,K., Tomancak,P., and Cardona,A. (2012). Fiji: an open-source platform for biological-image analysis. Nat. Methods *9*, 676-682.

Schmidt, M., Paes, K., De Mazière, A., Smyczek, T., Yang, S., Gray, A., French, D., Kasman, I., Klumperman, J., Rice, D.S., and Ye, W. (2007). EGFL7 regulates the collective migration of endothelial cells by restricting their spatial distribution. Development. *134*, 2913-23.

Sehnert,A.J., Huq,A., Weinstein,B.M., Walker,C., Fishman,M., and Stainier,D.Y. (2002). Cardiac troponin T is essential in sarcomere assembly and cardiac contractility. Nat. Genet. *31*, 106-110.

Soncin, F., Mattot, V., Lionneton, F., Spruyt, N., Lepretre, F., Begue, A., and Stehelin, D. (2003). VE-statin, an endothelial repressor of smooth muscle cell migration. EMBO J. *22,* 5700–11.

Song,Y., Eng,M., and Ghabrial,A.S. (2013). Focal defects in single-celled tubes mutant for Cerebral cavernous malformation 3, GCKIII, or NSF2. Dev. Cell *25*, 507-519.

Tanjore, H., Zeisberg, E.M., Gerami-Naini, B., and Kalluri, R. (2008). Beta1 integrin expression on endothelial cells is required for angiogenesis but not for vasculogenesis. Dev Dyn. *237*, 75-82.

Vermot,J., Forouhar,A.S., Liebling,M., Wu,D., Plummer,D., Gharib,M., and Fraser,S.E. (2009). Reversing blood flows act through klf2a to ensure normal valvulogenesis in the developing heart. PLoS. Biol. *7*, e1000246.

Villefranc,J.A., Amigo,J., and Lawson,N.D. (2007). Gateway compatible vectors for analysis of gene function in the zebrafish. Dev. Dyn. *236*, 3077-3087.

Voss,K., Stahl,S., Schleider,E., Ullrich,S., Nickel,J., Mueller,T.D., and Felbor,U. (2007). CCM3 interacts with CCM2 indicating common pathogenesis for cerebral cavernous malformations. Neurogenetics. *8*, 249-256.

Wang, S., Aurora, A.B., Johnson, B.A., Qi, X., McAnally, J., Hill, J.A., Richardson, J.A., Bassel-Duby, R., and Olson, E.N. (2008). The endothelial-specific microRNA miR-126 governs vascular integrity and angiogenesis. Dev Cell.*15*, 261-71.

Westerfield,M., Doerry,E., Kirkpatrick,A.E., Driever,W., and Douglas,S.A. (1997). An on-line database for zebrafish development and genetics research. Semin. Cell Dev. Biol. *8*, 477-488.

Whitehead,K.J., Chan,A.C., Navankasattusas,S., Koh,W., London,N.R., Ling,J., Mayo,A.H., Drakos,S.G., Jones,C.A., Zhu,W., Marchuk,D.A., Davis,G.E., and Li,D.Y. (2009). The cerebral cavernous malformation signaling pathway promotes vascular integrity via Rho GTPases. Nat. Med. *15*, 177-184.

Wustehube,J., Bartol,A., Liebler,S.S., Brutsch,R., Zhu,Y., Felbor,U., Sure,U., Augustin,H.G., and Fischer,A. (2010). Cerebral cavernous malformation protein

CCM1 inhibits sprouting angiogenesis by activating DELTA-NOTCH signaling. Proc. Natl. Acad. Sci. U. S. A *107*, 12640-12645.

Yoruk,B., Gillers,B.S., Chi,N.C., and Scott,I.C. (2012). Ccm3 functions in a manner distinct from Ccm1 and Ccm2 in a zebrafish model of CCM vascular disease. Dev. Biol. *362*, 121-131.

Yu,P.C., Gu,S.Y., Bu,J.W., and Du,J.L. (2010). TRPC1 is essential for in vivo angiogenesis in zebrafish. Circ. Res. *106*, 1221-1232.

Zawistowski,J.S., Serebriiskii,I.G., Lee,M.F., Golemis,E.A., and Marchuk,D.A. (2002). KRIT1 association with the integrin-binding protein ICAP-1: a new direction in the elucidation of cerebral cavernous malformations (CCM1) pathogenesis. Hum. Mol. Genet. *11*, 389-396.

Zawistowski,J.S., Stalheim,L., Uhlik,M.T., Abell,A.N., Ancrile,B.B., Johnson,G.L., and Marchuk,D.A. (2005). CCM1 and CCM2 protein interactions in cell signaling: implications for cerebral cavernous malformations pathogenesis. Hum. Mol. Genet. *14*, 2521-2531.

Zhang,J., Clatterbuck,R.E., Rigamonti,D., Chang,D.D., and Dietz,H.C. (2001). Interaction between krit1 and icap1alpha infers perturbation of integrin beta1-mediated angiogenesis in the pathogenesis of cerebral cavernous malformation. Hum. Mol. Genet. *10*, 2953-2960.

Zhang,J., Rigamonti,D., Dietz,H.C., and Clatterbuck,R.E. (2007). Interaction between krit1 and malcavernin: implications for the pathogenesis of cerebral cavernous malformations. Neurosurgery 60, 353-359.

Zheng,X., Xu,C., Di,L.A., Kleaveland,B., Zou,Z., Seiler,C., Chen,M., Cheng,L., Xiao,J., He,J., Pack,M.A., Sessa,W.C., and Kahn,M.L. (2010). CCM3 signaling through sterile 20-like kinases plays an essential role during zebrafish cardiovascular development and cerebral cavernous malformations. J. Clin. Invest 120, 2795-2804.

Zheng,X., Xu,C., Smith,A.O., Stratman,A.N., Zou,Z., Kleaveland,B., Yuan,L., Didiku,C., Sen,A., Liu,X., Skuli,N., Zaslavsky,A., Chen,M., Cheng,L., Davis,G.E., and Kahn,M.L. (2012). Dynamic regulation of the cerebral cavernous malformation pathway controls vascular stability and growth. Dev. Cell 23, 342-355.

Zhu,Y., Wu,Q., Xu,J.F., Miller,D., Sandalcioglu,I.E., Zhang,J.M., and Sure,U. (2010). Differential angiogenesis function of CCM2 and CCM3 in cerebral cavernous malformations. Neurosurg. Focus. 29, E1.

ACKNOWLEDGEMENTS

We would like to thank M. Affolter, M. Andrade, H. Belting, N. Chi, J. Essner, R. Fechner, M. Huska, N. Lawson, J. Mably, A. Maul, J. Richter, A. Siekmann, D. Stainier, U. Strähle, H.J. Tsai for providing reagents, fish stocks or other support. Thanks to Russ Hodge, Andreas Kispert, Francesca Spagnoli, and members of the Abdelilah-Seyfried lab for helpful comments and suggestions on the manuscript. We would like to thank the Confocal and 2-Photon Microscopy Core Facility (Max Delbrück Center for Molecular Medicine) staff, Anje Sporbert and Zoltan Cseresnyes, for their technical assistance and overall imaging support. U.F. was funded by the DFG (FE432/9-1) and EU (EnVision). C.A.-R., E.F., S.M.-D. and E. T.-L. are supported by two grants from the European consortium ERA-net NEURON. S.A.-S. was supported by a Heisenberg fellowship of the Deutsche Forschungsgemeinschaft (DFG). This work was supported by a fellowship of the Fritz Thyssen Foundation (10.07.2.128), DFG grant SE2016/7-1 and SE2016/7-2, support by the excellence cluster REBIRTH, and BayGene.

FIGURE LEGENDS

Fig. 1. Loss of CCM proteins causes elevated levels of *klf2* expression. (A-C) Loss of Ccm2 causes elevated levels of *klf2a* and *klf2b* mRNA in zebrafish at 48 hpf **(A)**, of *Klf2* mRNA in mouse cerebellar tissue of *iCCM2* mice at P15 **(B)**, and of *KLF2* mRNA in HUVECs **(C)** as determined by RT-qPCR. **(D-H)** At 48 hpf, whole-mount *in situ* hybridizations show that *klf2a* is misexpressed within the entire endocardium of *krit1*^{ty219c} and *ccm2*^{m201} mutants (D-F) and is elevated within arteries and veins in the tail region (asterisk) of *ccm2*^{m201} mutants (G-H). Statistical data are means and s.e.m.; *, p<0.05, **, p<0.01; ***, p<0.001; ****, p<0.0001; see supplemental information for details about statistical data analysis.

Fig. 2. Elevated levels of *klf2* mRNA cause morphogenetic defects in zebrafish *ccm* mutants. (A-I) Rescue of cardiac malformations, lateral dorsal aorta (LDA) defects, and subintestinal vein (SIV) defects in zebrafish *ccm2*^{m201} mutants (B,B',E,H) by targeting *klf2a*/*b* with MOs (C,C',F,I). **(A-C)** Shown are hearts of different genotypes at 48 hpf or (A',B',C') details with single confocal plane sections of the atrioventricular canal (AVC) region (arrowheads) (white box). Endocardial cushion cells are marked by Tg(*kdrl:GFP*)^{s843} and Alcam staining (asterisks). **(D-F)** Dorsal views of the LDA marked by Tg(*kdrl:GFP*)^{s843} (inverted images) in different genotypes at 48 hpf. **(G-I)** Side view of the SIV marked by Tg(*kdrl:GFP*)^{s843} in different genotypes at 72 hpf. Vessel branch point defects (arrows) within the SIV are reduced by targeting *klf2a/b* in *ccm2*^{m201} mutants (H,I). **(J)** Endocardial and LDA cell numbers are elevated in *ccm2*^{m201} mutants at 48 hpf, as well as upon overexpression of *klf2a* from a heat-shock

inducible promoter. **(K)** Quantifications of the number of branchpoints of the SIV in different genotypes at 72 hpf. **(L,M)** Endothelial overexpression of *klf2a* in Tg(*fli1ep:Gal4FF*)^{ubs2}; *Tg*(*UAS:KLF2a*)$^{ig1-3}$; *Tg*(*kdrl:GFP*)^{s843} transgenic embryos is sufficient to phenocopy the *ccm2*^{m201} mutant cardiac ballooning phenotype. endo, endocardium; myo, myocardium; A, atrium; V, ventricle. Scale bars are all 25µm. Statistical data are means and s.e.m.; ns, not significant; *, p<0.05; **, p<0.01; ***, p<0.001; ****, p<0.0001; see supplemental information for details about statistical data analysis.

Fig. 3. Enhanced VEGFR signaling is involved in the zebrafish *ccm2*^{m201} mutant cardiac phenotype. (A-C) Rescue of cardiac malformations in *ccm2*^{m201} mutants at 48 hpf after treatment with the VEGFR inhibitor PTK787 between 15-17 hpf. (A-C) Shown are hearts marked by endocardial Tg(*kdrl:GFP*)^{s843} and Actin staining at 48 hpf or (A',B',C') details with single confocal plane sections of the AVC region (white box in A,B,C). Endocardial cushion cells are characterized by their cuboidal shape and cortical Actin (asterisks) (n=5/5 genotyped *ccm2*^{m201} mutants completely rescued by PTK787 treatment). **(D)** Treatment of *ccm2*^{m201} mutants with PTK787 between 15-17 hpf significantly reduces the endocardial overproliferation phenotype and treatment between 24-48 hpf suppresses the overgrowth of the LDA. **(E)** The phenotypic rescue of *ccm2*^{m201} mutants by treatment with PTK787 between 15-48 hpf does not affect the elevated expression levels of *klf2a* and *klf2b* as detected by RT-qPCR. endo, endocardium; myo, myocardium. Scale bars are all 25µm. Statistical data are

means and s.e.m.; ns, not significant; *, p<0.05; **, p<0.01; ***, p<0.001; ****, p<0.0001; see supplemental information for details about statistical data analysis.

Fig. 4. Elevated expression levels of *egfl7* mRNA are involved in the *ccm2*^{m201} mutant phenotype. (A) Loss of Ccm2 or overexpression of *klf2a/b* in Tg(*hsp70l:klf2a_IRES_EGFP)*^{md8} or Tg(*hsp70l:klf2b_IRES_EGFP*)^{md9} transgenic embryos causes elevated levels of *egfl7* mRNA as determined by RT-qPCR. **(B)** Similarly, *EGFL7* is upregulated in HUVECs upon knock-down of *ICAP1*, *KRIT1*, or *CCM2* by siRNA treatment. **(C-E')** Cardiac morphology and cardiac cushion formation are rescued by *egfl7* MO injection (n=15/15 genotyped *ccm2*^{m201} mutants completely rescued by *egfl7* MO). Shown are hearts marked by endocardial Tg(*kdrl:GFP*)^{s843} and Actin staining at 48 hpf or (C'-E') details with single confocal plane sections of the AVC region. Endocardial cushion cells are marked by the expression of Alcam (inverted image) (asterisks). Scale bars are all 25µm. Statistical data are means and s.e.m.; *, p<0.05; **, p<0.01; ***, p<0.001; see supplemental information for details about statistical data analysis.

Fig. 5. Blood flow-independent expression of *klf2a*/*b* mRNA in *ccm2*^{m201} mutants. (A-C) The *ccm2*^{m201} mutant cardiac ballooning phenotype is flow-independent. Frontal views of 48hpf hearts of the myocardial reporter line Tg(*myl7:GFP*)^{twu34} (Huang et al., 2003) show that cardiac expansion is not rescued in *ccm2*^{m201} mutant; *tnnt2a* morphants that lack blood flow. **(D)** The expression levels of *klf2a* and *klf2b* mRNA as measured by RT-qPCR are elevated in *ccm2*^{m201} mutant; *tnnt2a* morphants that lack blood flow. **(E-G)** Loss of Ccm2 results in overproliferation of the endocardium under no-flow conditions.

(E) Quantifications of the ratio of proliferating versus non-proliferating endocardial cells between 33-53 hpf in *tnnt2a* morphants compared with *ccm2*^{m201} mutant;*tnnt2a* morphants based on SPIM recordings (n=2). **(F)** The endocardium of *tnnt2a* morphants is not proliferative as indicated by the lack of color-coded proliferative cells [still image derived from supplementary movie S1, which is based on SPIM timelapse recordings of endocardial morphogenesis marked by Tg(*kdrl:GFP*)^{s843} between 33-53 hpf]. **(G)** The combined loss of Ccm2 and Tnnt2a is characterized by a high rate of proliferative events (indicated by uniquely colored daughter cells derived from proliferative events; still image derived from supplementary movie S2). A, atrium; V, ventricle. Statistical data are means and s.e.m.; ns, not significant; *, p<0.05; **, p<0.01; ***, p<0.001; ****, p<0.0001; see supplemental information for details about statistical data analysis.

Fig. 6. Misexpression of *KLF2* depends on integrin β1. (A) RT-qPCR shows that elevated expression of *KLF2* mRNA in *ICAP1*-, *KRIT1*-, or *CCM2*-silenced HUVECs is partly suppressed upon simultaneously interfering with *β1 integrin* (*ITGB1*). **(B-D)** Morpholino knockdown of zebrafish *integrinβ1b* completely restores cardiac morphology [marked by Tg(*kdrl:GFP*)^{s843} and Actin staining] and cardiac cushion formation in zebrafish *ccm2*^{m201} mutants at 48hpf. (B'-D') Shown are single confocal plane sections with details of the atrioventricular canal (AVC) region (white box in B-D) with endocardial cushion cells are marked by Alcam (asterisks). **(E)** Model of CCM/ICAP1 controlled proangiogenic activity of the β1 integrin-Klf2 mechanotransduction pathway. endo, endocardium; myo, myocardium. Scale bars are all 25μm. Statistical data are means and s.e.m.; ns,

not significant;***, p<0.001; ****, p<0.0001; see supplemental information for details about statistical data analysis.

Table 1: Upregulation of angiogenesis-related gene expression in *ccm2*^{m201} mutants. List of angiogenesis-related genes up-regulated in *ccm2*^{m201} cardiac tissue at 72hpf compared with wild-type. The two *klf2* homologous genes are marked in grey.

Figure

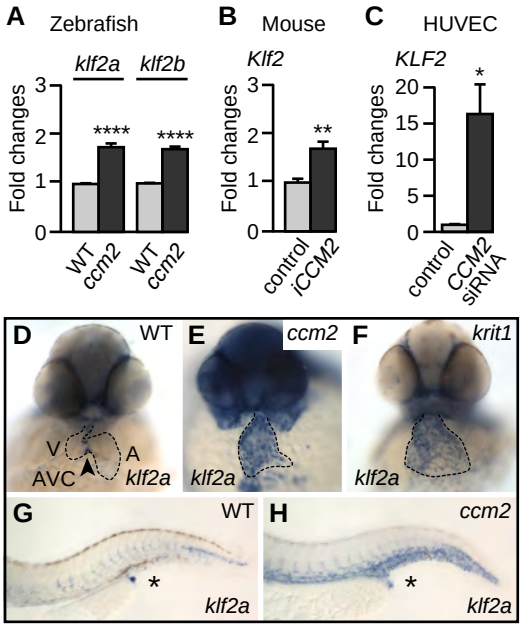

Figure 1
Renz et al., 2014

Figure

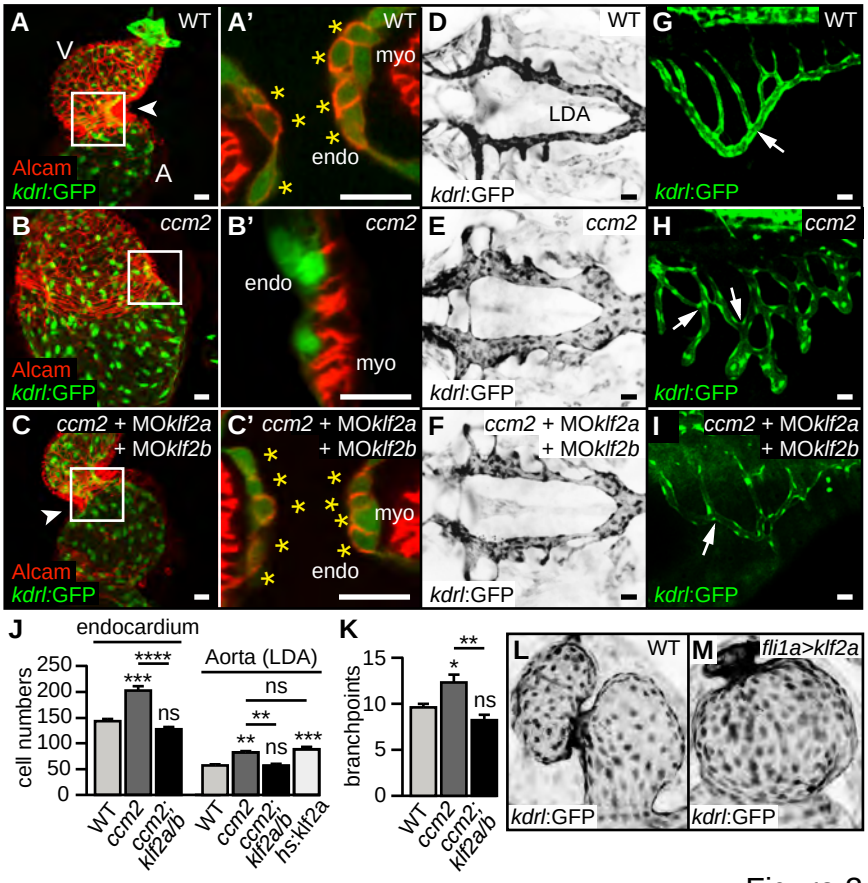

Figure 2
Renz et al., 2014

Figure

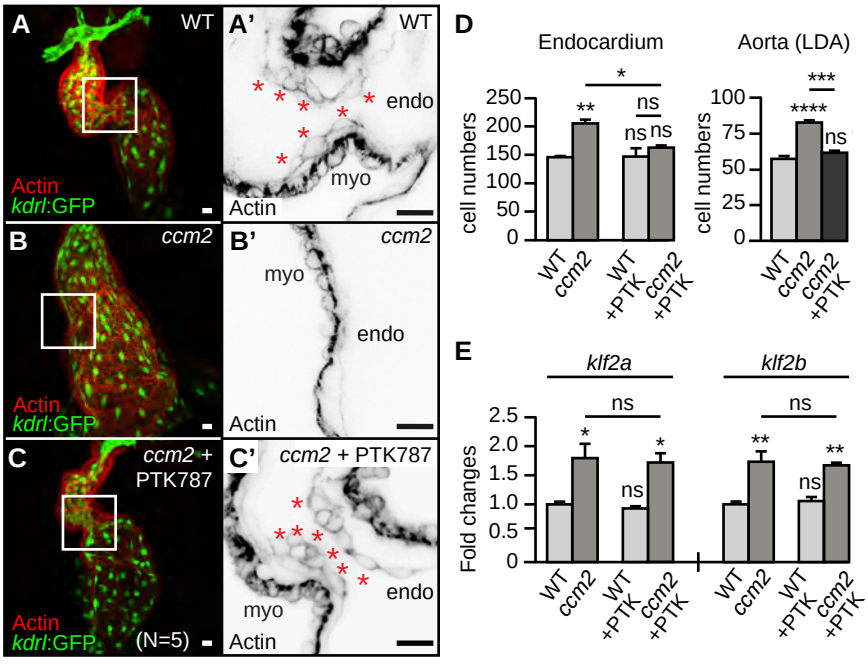

Figure 3
Renz et al., 2014

Figure

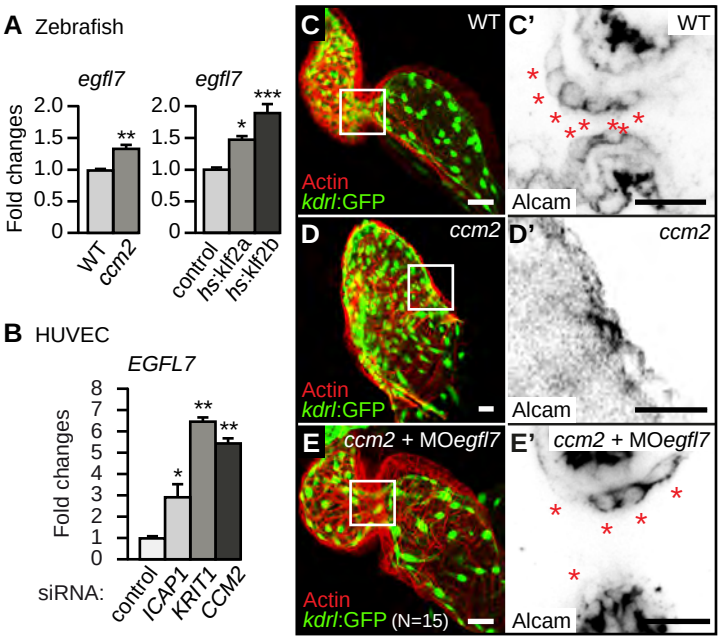

Figure 4
Renz et al., 2014

Figure

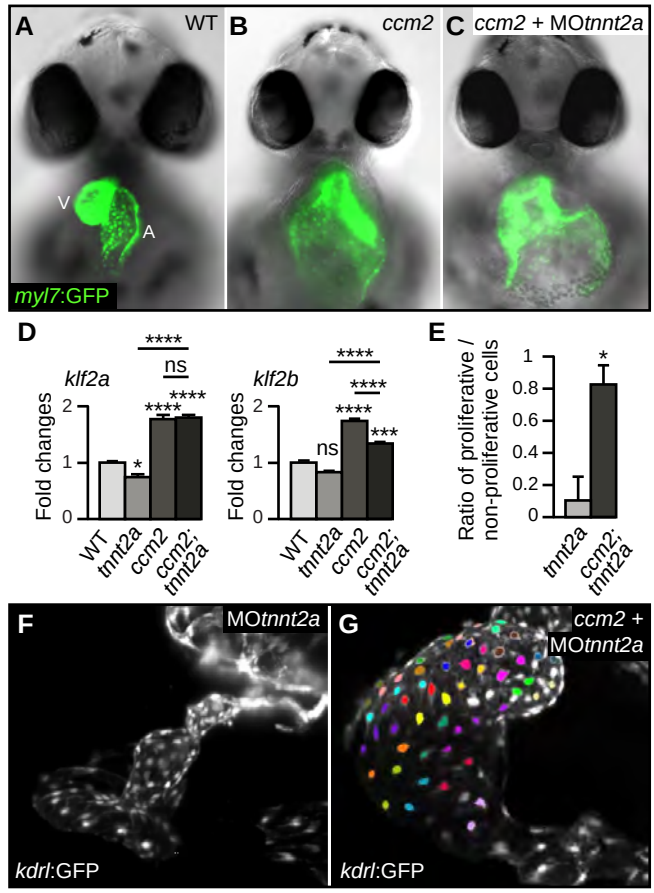

Figure 5
Renz et al., 2014

Figure

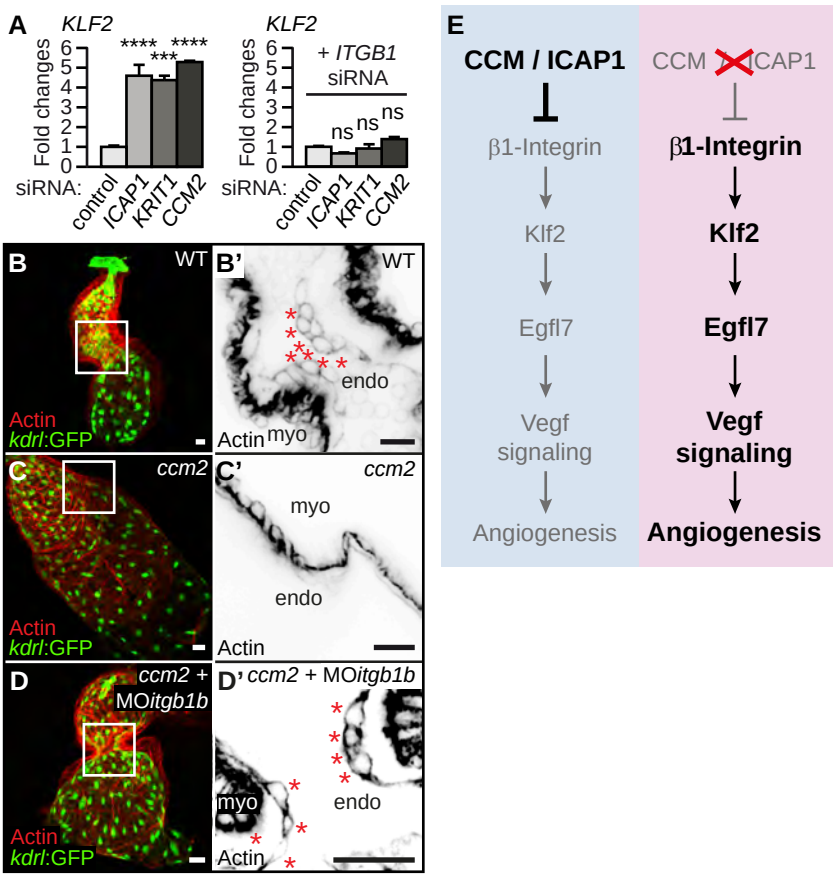

Figure 6
Renz et al. 2014

Table

Agilent Probe	Dr Gene	Hs Ortholog	$\log_2$ fold change
A_15_P105948	*nrp2b*	*NRP2*	2.034
A_15_P119736	*klf2b*	*KLF2*	1.887
A_15_P108040	*klf2a*	*KLF2*	1.587
A_15_P162576	*egfl7*	*EGFL7*	1.369
A_15_P103182	*nrp2a*	*NRP2*	1.074
A_15_P178471	*flt1*	*FLT1*	1.038
A_15_P111146	*vegfc*	*VEGFC*	0.971
A_15_P133286	*kdr*	*KDR*	0.894
A_15_P150091	*fli1b*	*FLI1*	0.789
A_15_P195331	*flt4*	*FLT4*	0.778

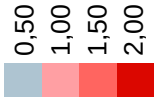

Table 1
Renz et al., 2014

INVENTORY OF SUPPLEMENTAL INFORMATION

1. Figs. S1 to S5
2. Movies 1-3
3. Experimental Procedures
4. References for Experimental Procedures

- Figure S1, related to Figure 1, shows endocardial misexpression of *klf2b* in *krit1*^{ty219c} and *ccm2*^{m201} mutants (related to main Figure 1D-F).
- Figure S2, related to Figure 2, shows that the cardiac malformation phenotypes in *ccm2*^{m201}, *krit1*^{ty219c}, and *heg*^{m552} mutants are rescued by targeting *klf2a/b* with MOs. Targeting of either *klf2a* or *klf2b* in *ccm2*^{m201} mutants does not rescue cardiac phenotypes (related to main Figure 2A-C).
- Figure S3, related to Figure 4, shows that coinjection of *egfl7* and *klf2a/b* morpholinos rescues the cardiovascular phenotype of *ccm2*^{m201} mutants.
- Figure S4, related to Figure 4, shows that *miR-126a* and *miR-126b* levels are unchanged in *ccm2*^{m201} mutants.
- Figure S5, related to Figure 6, shows that siRNA treatment in HUVECs efficiently lowers protein levels of CCM2, KRIT1, ICAP1, or ITGB1, respectively.
- Movies 1 and 2, related to main Figure 5, are selective plane illumination microscopy timelapse movies of endocardial development between 33-53hpf in *tnnt2a* morphants that lack blood flow (Movie 1) and *tnnt2a* morphants;*ccm2*^{m201} mutants (Movie 2) (related to Figure 5E-G).
- Movie 3, related to Figure 5, is a microangiography of a human brain with a cavernous malformation and shows that the cavernoma region is characterized by low blood perfusion.

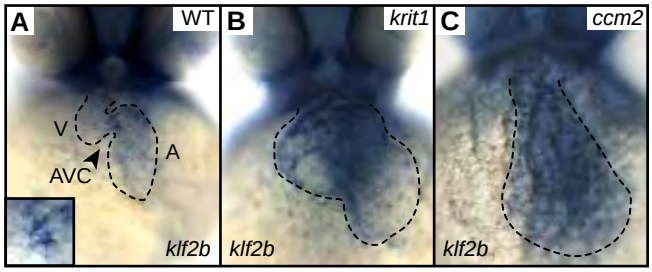

Figure S1

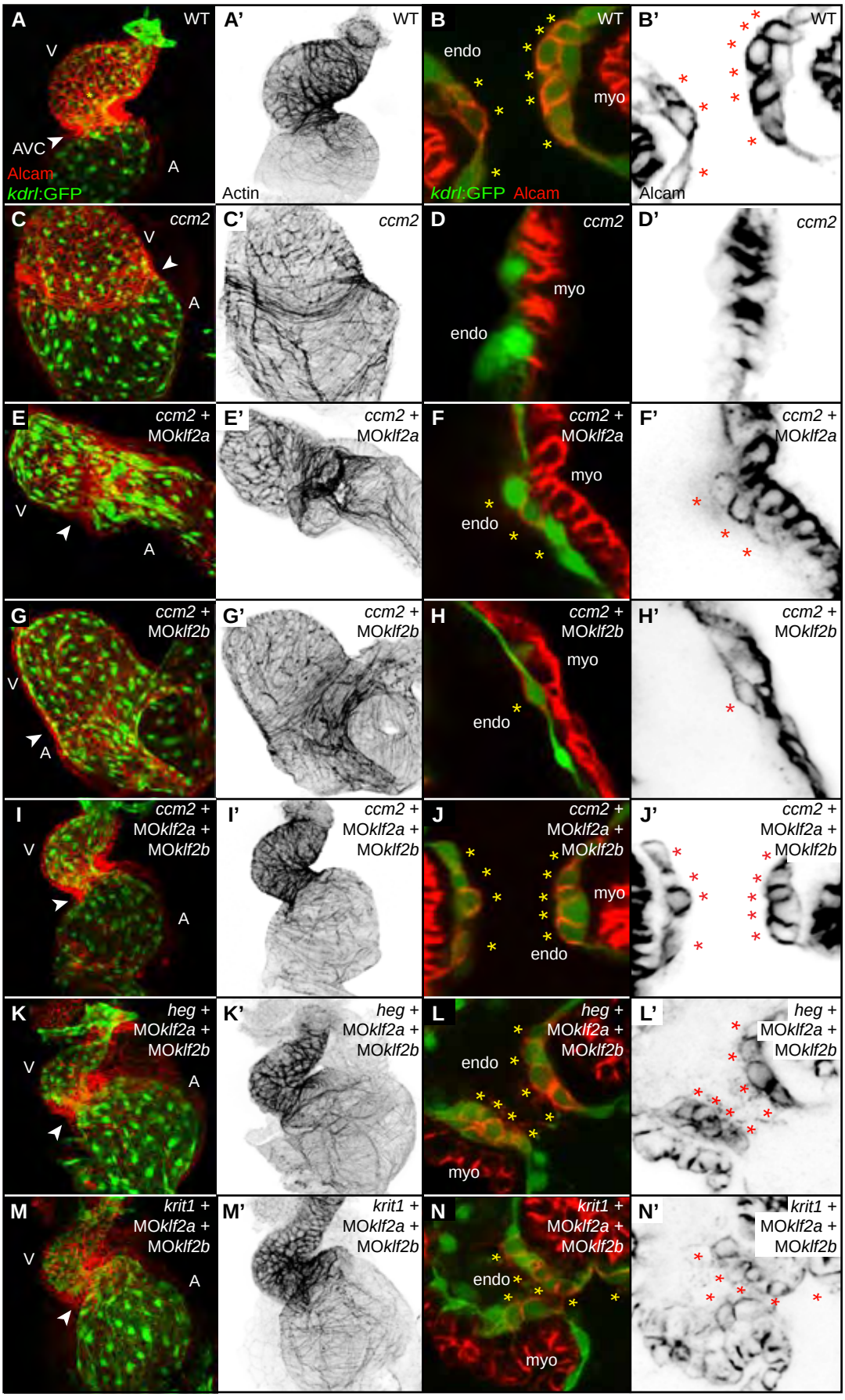
A
WT
V
AVC
A
Alcam
kdrl:GFP
A'
WT
Actin
B
WT
endo
myo
kdrl:GFP Alcam
B'
WT
Alcam
C
ccm2
V
A
C'
ccm2
D
ccm2
myo
endo
D'
ccm2
E
ccm2 +
MOklf2a
V
A
E'
ccm2 +
MOklf2a
F
ccm2 +
MOklf2a
myo
endo
F'
ccm2 +
MOklf2a
G
ccm2 +
MOklf2b
V
A
G'
ccm2 +
MOklf2b
H
ccm2 +
MOklf2b
myo
endo
H'
ccm2 +
MOklf2b
I
ccm2 +
MOklf2a +
MOklf2b
V
A
I'
ccm2 +
MOklf2a +
MOklf2b
J
ccm2 +
MOklf2a +
MOklf2b
myo
endo
J'
ccm2 +
MOklf2a +
MOklf2b
K
heg +
MOklf2a +
MOklf2b
V
A
K'
heg +
MOklf2a +
MOklf2b
L
heg +
MOklf2a +
MOklf2b
endo
myo
L'
heg +
MOklf2a +
MOklf2b
M
krit1 +
MOklf2a +
MOklf2b
V
A
M'
krit1 +
MOklf2a +
MOklf2b
N
krit1 +
MOklf2a +
MOklf2b
endo
myo
N'
krit1 +
MOklf2a +
MOklf2b

Figure S2

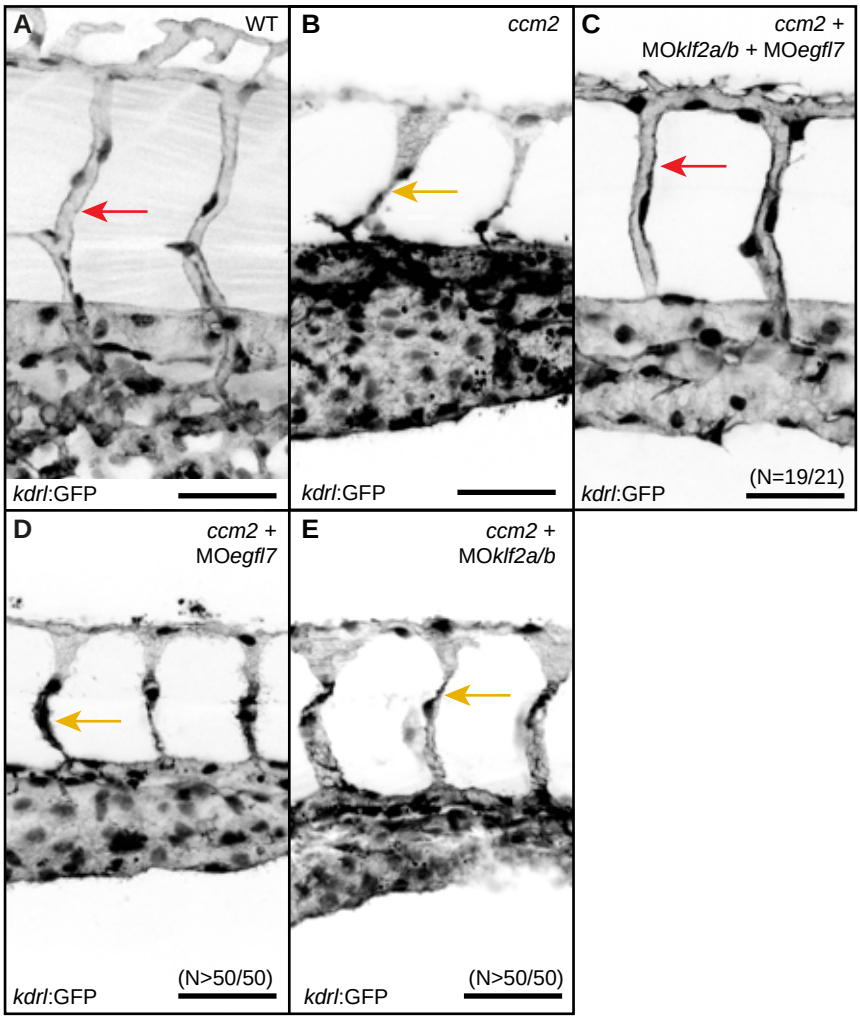
A
WT
kdrl:GFP
B
ccm2
kdrl:GFP
C
ccm2 +
MOklf2a/b + MOegfl7
(N=19/21)
kdrl:GFP
D
ccm2 +
MOegfl7
(N>50/50)
kdrl:GFP
E
ccm2 +
MOklf2a/b
(N>50/50)
kdrl:GFP

Figure S3

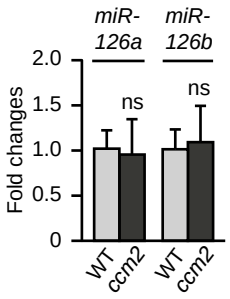
miR-126a
miR-126b
2.0
1.5
1.0
0.5
0
Fold changes
ns
ns
WT
ccm2
WT
ccm2

Figure S4

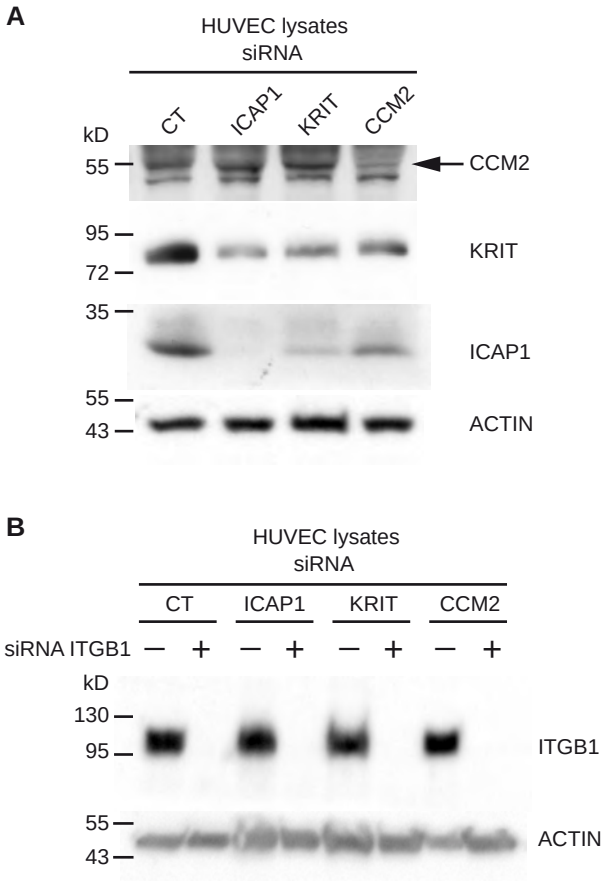
A
HUVEC lysates
siRNA
CT
ICAP1
KRIT
CCM2
kD
55
CCM2
95
72
KRIT
35
ICAP1
55
43
ACTIN
B
HUVEC lysates
siRNA
CT
ICAP1
KRIT
CCM2
siRNA ITGB1 – + – + – + – +
kD
130
95
ITGB1
55
43
ACTIN

Figure S5

1. SUPPLEMENTARY FIGURES

Fig. S1. Endocardial expression of *klf2b* mRNA is misregulated in zebrafish *ccm* mutants. (A) Whole-mount *in situ* hybridization reveals that *klf2b* is expressed at the atrioventricular canal (AVC) at 48 hpf in WT. **(B,C)** Loss of Krit1 or of Ccm2 causes elevated expression of *klf2b* throughout the entire ballooning endocardium.

Fig. S2. Rescue of cardiac cushions in *ccm2*^{m201} , *heg*^{m552}, and *krit1*^{ty219c} mutants by knockdown of Klf2a/b. (A,C,E,G,I,K,M) Shown are hearts of different genotypes marked by the endothelial reporter line Tg(*kdrl:GFP*)^{s843} counterstained with Alcam, or Actin staining alone (inverted image). **(B,D,F,H,J,L,N)** Details show single confocal planes of the atrioventricular canal (AVC) region. Endocardial cushion cells (asterisks) are marked by Tg(*kdrl:GFP*)^{s843} and Alcam staining, or Alcam staining only (inverted images). Whereas knockdown of only Klf2a (E,F) or Klf2b (G,H) does not rescue cardiac morphogenesis or the number of endocardial cushions cells in *ccm2*^{m201} mutants, knockdown of both Klf2 proteins completely restores cardiac morphology and cardiac cushion formation (I,J). **(K-N)** Similarly, *heg*^{m552} and *krit1*^{ty219c} mutants are completely rescued by the knockdown of Klf2a/b (n=5/5 of either mutant completely rescued). endo, endocardium; myo, myocardium; A, atrium; V, ventricle.

Fig. S3. Klf2a/b and Egfl7 interact to regulate lumen formation of intersegmental blood vessels. Compared to wild-type (A), the intersegmental vessels of *ccm2*^{m201} mutants (B) are not lumenized. Injection of *ccm2*^{m201} mutants with low doses of *egfl7* MO (D; n>50/50) or *klf2a/b* MO (E; n>50/50) does not rescue the lumenization defects within intersegmental vessels. In contrast, co-injection of *klf2a/b* MOs and *egfl7* MO into *ccm2*^{m201} mutants (C) completely rescues lumenization defects (n=19/21 mutants identified by genotyping). Red arrows: lumenized intersegmental vessels; orange arrows: non-lumenized intersegmental vessels. Scale bars are all 50µm.

Fig. S4. *miR-126a* and *miR-126b* are normally expressed in *ccm2*^{m201} mutants. RT-qPCR experiments revealed that neither *miR-126a* nor *miR-126b* levels are significantly changed in *ccm2*^{m201} mutant embryos at 48hpf. Statistical data are means and s.e.m.; ns, not significant; see supplemental information for details about statistical data analysis.

Fig. S5. Western blot analysis of CCM protein levels in HUVECs upon siRNA silencing. CCM2, KRIT1 and ICAP1 protein levels are reduced upon CCM2, KRIT1 and ICAP1 siRNA treatment, respectively. Similarly, ITGB1 levels are reduced upon ITGB1 siRNA treatment. Actin levels are shown as a loading control.

2. SUPPLEMENTARY MOVIES

Supplementary Movie 1. Selective plane illumination microscopy (SPIM) timelapse movie of zebrafish endocardial cell proliferation under no-blood flow conditions between 33-53 hpf. Selective plane illumination microscopy (SPIM) timelapse movie shows that the knockdown of Tnnt2a, which causes no-flow conditions within the heart, is characterized by low levels or no proliferation as indicated by the endothelial reporter line Tg(*kdrl:GFP*)^{s843} (see Figure 5E,F).

Supplementary Movie 2. Selective plane illumination microscopy (SPIM) timelapse movie of zebrafish endocardial cell proliferation under no-blood flow conditions and loss of Ccm2 between 33-53 hpf. Combined knockdown of Ccm2 and Tnnt2a results in a high rate of proliferative events as indicated by the endothelial reporter line Tg(*kdrl:GFP*)^{s843}. Nuclei of proliferative cells are color coded during mitosis and remain uniquely colored throughout the recording (see Figure 5E,G).

Supplementary Movie 3. Angiography of human brain with a cavernous malformation. Perfusion with a contrast reagent shows that the cavernoma region is characterized by low blood perfusion.

3. SUPPLEMENTARY EXPERIMENTAL PROCEDURES

Gateway cloning of transgenesis constructs. The open reading frames of zebrafish *klf2a* (NM_131856) (Vermot et al., 2009) or zebrafish *klf2b* (NM_131857) were amplified by PCR and cloned into the Gateway pDONR 221 vector (Kwan et al., 2007; Villefranc et al., 2007) (referred to as pME-*klf2a* or pME-*klf2b*; primer sequences available upon request). The following final constructs were generated by standard Gateway cloning reactions with pDestTol2, p5E-UAS or p5E-*hsp70l*, pME-*klf2a* or pME-*klf2b*, and p3E-pA or p3E-*IRES_EGFP*:

UAS:klf2a

hsp70l:klf2a_IRES_EGFP

hsp70l:klf2b_IRES_EGFP

Generation of transgenic lines of zebrafish. Each of the transformation plasmids was coinjected with the Tol2 transposase capped mRNA synthetised using the SP6 polymerase (mMessage Machine, Ambion) into one-cell stage zebrafish embryos. Several independent transgenic lines were established for each construct. In functional tests, these independent lines resulted in comparable phenotypes.

Zebrafish lines and handling. Handling of zebrafish was done in compliance with German and Berlin state law, carefully monitored by the local authority for animal protection (LaGeSo, Berlin-Brandenburg, Germany). The following strains were maintained under standard conditions as previously described (Westerfield et al., 1997): *ccm2*^{m201} (Mably et al., 2006), *krit1*^{ty219c} (Mably et al., 2006), *heg*^{m552} (Mably et al., 2003), Tg(*myl7:GFP*)^{twu34} (Huang et al., 2003), Tg(*kdrl:GFP*)^{s843} (Jin et al., 2005), Tg(*fli1a:GAL4FF*)^{ubs2} (Herwig et al., 2011), Tg(*UAS:klf2a*)$^{ig1-3}$, Tg(*hsp70l:klf2a_IRES_EGFP*)^{md8}, Tg(*hsp70l:klf2b_IRES_EGFP*)$^{md9-11}$.

Heat-shock experiments. For the experiment shown in Fig. 2J, Tg(*hsp70l:klf2a_IRES_EGFP*)^{md8} embryos were heat-shocked three times: at the 11-somite stage (30min at 37°C), then at 24hpf (40min at 38°C), and at 40hpf (45min at 38°C). Alternatively, for the experiment shown in Fig. 4A, Tg(*hsp70l:klf2a_IRES_EGFP*)^{md8} and Tg(*hsp70l:klf2b_IRES_EGFP*)^{md9} embryos were heat-shocked only once at 24hpf (40min at 38°C) .

Morpholino injections. Embryos were injected at the one-cell stage with the following morpholinos as previously described:

morpholino name	morpholino sequence	Amount / embryo	Ref.
klf2a ATG	5‘-GGACCTGTCCAGTTCATCCTTCCAC-3‘	12ng	(Nicoli et al., 2010)
klf2b ATG	5‘-AAAGGCAAGGTAAAGCCATGTCCAC-3‘	12ng	-
5ng *klf2a*MO + 5ng *klf2b*MO			
egfl7 ATG	5‘-CAGGTGTGTCTGACAGCAGAAAGAG-3‘	650pg	(Parker et al., 2004)
2,5ng *klf2a*MO + 2,5ng *klf2b*MO + 0,3ng *egfl7*MO			
tnnt2a ATG	5‘-CATGTTTGCTCTGATCTGACACGCA-3‘	2ng	(Sehnert et al., 2002)
itgb1b splice	5‘-GCCAGTTTGAGTGAATAACTCACCT-3‘	6.3ng	(Ablooglu et al., 2010)

Pharmacological treatment. Embryos were treated in E3 medium with 12,5μM of VEGFR inhibitor PTK787 (Chan et al., 2002). Control embryos were treated with 0,01% DMSO. Treatment protocols corresponding with different figures were as follows:

1). between 15-17hpf (shown in Fig. 3C,C’; Fig. 3D – only endocardium)

2). between 24-48hpf (shown in Fig. 3D – only LDA; Fig. 3E)

Immunohistochemistry. Zebrafish whole-mount immunohistochemistry was performed on 48 hpf embryos as previously described (Veerkamp et al., 2013) The following antibodies were used: mouse Zn-8/Alcam (1:100; Developmental Studies Hybridoma Bank)(Beis et al., 2005); Cy5-conjugated secondary antibody goat-anti-mouse (1:250; Jackson ImmunoResearch Laboratories cat# 96829); Rhodamine Phalloidine was incubated in combination with the secondary antibody to stain Actin (1:100; Sigma cat# 658740). Images were recorded at a LSM710 confocal microscope (Zeiss) and processed with Adobe Photoshop (Adobe Systems).

Statistical analysis of endocardial and lateral dorsal aorta cell numbers. In Figure 2J and Figure 3D, nuclei were visualized by Tg(*kdrl:GFP*)^{s843} expression and were counted within the heart (for endocardium), or in both lateral dorsal aortae in an area defined between the branching point from the dorsal aorta and the branching point of the first aortic arch. Cell numbers are shown as means with S.E.M. Prism 5 (GraphPad) was

used to perform 1-way ANOVA tests followed by Sidak's multiple comparisons tests (Fig. 2J, 3D). Means are statistically significantly different when $P < 0.05$.

	Endocardium n=	Average cell number	S.E.M.
WT	3	144,7	1,202
WT + PTK787	3	146,7	14,52
ccm2	3	205,3	6,692
ccm2 + PTK787	4	162,5	3,797
ccm2;*klf2ab*MO	3	131	2,082

	1-way ANOVA	P value
Fig. 2J, endocardium	wt vs *ccm2*	*** P=0,0001
	wt vs *ccm2*;*klf2ab*MO	n.s. P=0,1607
	ccm2 vs *ccm2*;*klf2ab*MO	**** P<0,0001
Fig. 3D, endocardium	wt vs *ccm2*	** P=0,0022
	wt vs wt + PTK787	n.s. P>0.9999
	wt vs *ccm2* + PTK787	n.s. P=0,4871
	wt + PTK787 vs *ccm2* + PTK787	n.s. P=0,5999
	ccm2 vs *ccm2* + PTK787	* P=0,0141

	LDA n=	Average cell number	S.E.M.
WT	3	57,6	1,453
ccm2	3	83	1,528
ccm2;*klf2ab*MO	2	56,5	3,5
*hsp70l:*klf2a	2	88,5	4,5
ccm2 + PTK787	3	62	1,53

	1-way ANOVA	P value
Fig.2J, LDA	wt vs *ccm2*	** P=0,0011
	wt vs *ccm2*;*klf2ab*MO	n.s. P=0,9991
	wt vs *hsp70l:klf2a*	*** P=0,0007
	ccm2 vs *hsp70l:klf2a*	n.s. P=0,6158
	ccm2 vs *ccm2*;*klf2ab*MO	** P=0,0015
Fig.3D, LDA	wt vs *ccm2*	**** P<0,0001
	wt vs *ccm2* + PTK787	n.s. P=0,2405
	ccm2 vs *ccm2* + PTK787	*** P=0,0002

Statistical analysis of subintestinal vein (SIV) branchpoints. In Figure 2K, SIV were visualized at 72 hpf by Tg(*kdrl:GFP*)^{s843} expression and branchpoints were counted.

Branchpoint numbers are shown as means with S.E.M. Prism 5 (GraphPad) was used to perform a 1-way ANOVA test followed by Sidak's multiple comparisons test. Means are statistically significantly different when $P < 0.05$.

	n=	Average number of branchpoints	S.E.M.
WT	10	9,6	0,371
ccm2	10	12,3	0,882
ccm2;*klf2ab*MO	5	8,2	0,583

	1-way ANOVA	P value
Fig. 2K	wt vs *ccm2*	* P=0,0198
	wt vs *ccm2*;*klf2ab*MO	n.s. P=0,5214
	ccm2 vs *ccm2*;*klf2ab*MO	** P=0,0036

Whole-mount *in situ* hybridizations. Zebrafish embryos were collected at 48hpf and fixed with 4% paraformaldehyde overnight at 4°C. The *klf2a* and *klf2b* antisense mRNA *in situ* probes were generated by PCR amplification from 24hpf WT cDNA (primers available upon request). The amplicons were cloned into the pSC-B vector with the StrataClone Blunt PCR Cloning kit (Stratagene). Antisense RNA was synthesized using the DIG RNA Labeling kit (Roche). *In situ* hybridization was performed as described elsewhere (Jowett and Lettice, 1994). After staining, the embryos were dehydrated in Benzylbenzoate and mounted in Permount for imaging. Images were recorded at an Axioplan2 microscope (Zeiss) and processed with Adobe Photoshop software (Adobe Systems).

HUVECs cell culture and transfection. HUVEC were obtained from Lonza and grown in EBM-2 media supplemented with 100U/ml penicillin / 100 µg/ml streptomycin at 37°C in a 5% CO_2-humidified chamber according to manufacturer's instructions. HUVEC ($1.5x10^6$ cells) were transfected twice at 24h interval with 20 nM siRNA and 45 µl lipofectamine RNAi max (Invitrogen) according to manufacturer's instructions. Cells were used the day after the second round of transfection. For silencing of *ß1 integrin*, at least 3 rounds of transfection were performed. Control conditions are mock transfections. *KRIT1* and *ITGB1* siRNA are siGENOME smart pool (Dharmacon) and *CCM2* siRNA is

ON-TARGET smart pool (Dharmacon*). ICAP-1* custom siRNA (Eurogentec) sequence is GCAUGCUCUCUACUUAAUA.

Western blot analysis of CCM proteins content in HUVECs upon siRNA silencing. siRNA transfected HUVEC were lysed in laemmli buffer the day after the last round of transfection, run on SDS-PAGE and transferred on PVDF membrane. Immunological detection was achieved as in Faurobert et al. (2013). Peroxidase activity was visualized by ECL (Clarity, BIORAD laboratories) using a ChemiDoc MP imaging system (BIORAD laboratories).

***iCCM2* mice.** Endothelial-specific conditional CCM2 knock-out mice *Cadh5(PAC)*-CreERT2/+; *Ccm2* $^{Fl/Del.}$, referred to as *iCCM2*, were treated with Tamoxifen at post-natal day 1 (P1) to induce the endothelial specific deletion of Ccm2 (Boulday et al., 2009). *Cadh5(PAC)*-CreERT2/+ mice were treated identically and used as controls. Mice were sacrificed at P15, the brains were prepared, snap-frozen, and the cerebella (in *iCCM2* mice, these harbor cavernomas) were subsequently isolated for RNA extraction.

Quantitative RT-qPCR for *miR-126a/b* in zebrafish. Total RNA was isolated from 50 – 100 whole zebrafish embryos 48 hours post fertilization using Trizol (Invitrogen). For reverse transcription reaction 1µg total RNA was used in miScript RT-kit purchased from Qiagen. RT-qPCR Primers specific for *miR-126a* (MSC0074644) and *miR-126b* (MSC0074645) were purchased from Qiagen and RT-PCR was performed using the miScript SYBR Green PCR Kit (Qiagen). RNU6 was used to normalize the *miR-126a/b* levels.

Quantitative RT-qPCR. RT-qPCR experiments were performed on zebrafish whole embryos, on P15 mouse cerebella, and on HUVECs in compliance with the MIQE standard (Bustin et al., 2009). For zebrafish, up to 25 embryos were pooled for each condition at 48hpf, or at 30hpf (in the case of heat-shocked fish; Fig. 4A). Zebrafish tissues were collected several times from independent experiments and therefore represent biological replicates. For the RT-qPCR experiment performed with *iCCM2* mouse tissues shown in Fig. 1B, total mRNA was extracted with Trizol (Sigma) from the cerebella of 5 mice per group. For mouse and zebrafish samples, cDNA was synthesized from total RNA with Moloney murine leukemia virus reverse transcriptase

(Invitrogen) using random hexamer nucleotides, and RT-qPCR experiments were performed as described (Veerkamp et al., 2013) using 6ng cDNA. The amplicon size was verified on agarose gels. For HUVECs, quantitative real-time PCR was performed with iTaqTM Universal SYBR Green Supermix (Bio-Rad) in a 25 µl reaction on a C-1000 Touch Thermal Cycler (BIORAD). Product sizes were controlled by DNA gel electrophoresis and the melt curves were evaluated using the BioRad CFX Manager. Ct-values were determined with the same software. The following primers were used for RT-qPCR:

	Primer name	Primer sequence	UniGene identifier
human	For_KLF2 Rev_KLF2	5‘-CATCTGAAGGCGCATCTG-3‘ 5‘-CGTGTGCTTTCGGTAGTGG-3‘	Hs.744182
	For_EGFL7 Rev_EGFL7	5‘-GTGGACCTGCTGGAGGAGAA-3‘ 5’-TCCGGGAGCCCATGCT-3’	Hs.91481
	For_ATP5O Rev_ATP5O	5‘-ATTGAAGGTCGCTATGCCACAG-3‘ 5‘-AACAGAAGCAGCCACTTTGGG-3‘	Hs.409140
mouse	Klf2Mm_fwd Klf2Mm_rev	5‘-AGGAGCGCTGGCCGCGAAAT-3‘ 5‘-GGCGCCCAGACCGTCCAATC-3‘	Mm.26938
	Eif1Mm_fwd Eif1Mm_rev	5‘-ATGGTACTGTAATTGAGCATCC-3‘ 5‘-GTGACAAGGGACAGAAGGGAAA-3‘	Mm.13886
zebrafish	Klf2aDr_fwd Klf2aDr_rev	5‘-CTGGGAGAACAGGTGGAAGGA-3‘ 5‘-CCAGTATAAACTCCAGATCCAGG-3‘	Dr.29173
	Klf2bDr_fwd Klf2bDr_rev	5‘-GGATAGATGGAAGATTGAGGAGCA-3‘ 5‘-CTCCAGGTCTAAATAATTGCTGAG-3‘	Dr.9976
	Egfl7_fwd Egfl7_rev	5‘-TTTACCCAGAATGCTGTCCG-3‘ 5‘-AAAACTGCCCAGCGTATTCA-3‘	Dr.89996
	Eif1bDr_fwd Eif1bDr_rev	5‘-CAGAACCTCCAGTCCTTTGATC-3‘ 5‘-GCAGGCAAATTTCTTTTTGAAGGC-3‘	Dr.162048

RT-qPCR data analyses. Results were analyzed using the comparative threshold cycle (Ct) method ($2^{-\Delta\Delta Ct}$) to compare gene expression levels between samples as previously described (Livak and Schmittgen, 2001). As internal reference genes, we used zebrafish *eif1b,* mouse *EIF1*, and for HUVECs normalization was done with the house keeping genes *GAPDH*, *RELA* or *ATP5O*, yielding comparable results. Expression levels of each target gene in the siRNA –treated HUVECs were calculated with *ATP5O* as reference gene and compared to control. The RT-qPCR experiments with HUVECs shown in Figure 1C were performed 4 times; the results of the RT-qPCR experiments shown in

Figure 4B and 6A are representative of more than 3 experiments. The mRNA expression levels of *klf2a, klf2b, egfl7* (zebrafish), *Klf2* (mouse), and *KLF2* (HUVECs) are shown as relative mean values with S.E.M. The statistical analysis was done with Prism 5 (GraphPad) to perform unpaired t-tests (zebrafish in Fig. 1A, 4A; mouse in Fig. 1B), a paired t-test (HUVECs in Fig. 1C), 1-way ANOVA tests followed by Sidak's multiple comparisons tests (zebrafish in Fig. 3E, 5D), or 1-way ANOVA tests with Dunnett's Multiple Comparison Test (zebrafish in Fig. 4A, HUVECs in Fig. 4B and 6A). Means are statistically significantly different if $P < 0.05$.

zebrafish		n=	*klf2a*		*klf2b*		*egfl7*	
			Mean	SEM	Mean	SEM	Mean	SEM
Fig. 1A	wt	4	1,002	0,033	1,004	0,052	-	-
	ccm2	5	1,779	0,073	1,740	0,046	-	-
Fig. 3E	wt	3	1,001	0,029	1,002	0,043	-	-
	ccm2	3	1,796	0,248	1,725	0,173	-	-
	wt + PTK787	3	0,925	0,030	1,054	0,062	-	-
	ccm2 + PTK787	3	1,713	0,163	1,666	0,039	-	-
Fig. 4A	wt	3	-	-	-	-	1	0,017
	ccm2	3	-	-	-	-	1,335	0,070
Fig. 4A	Heat-shock control	3	-	-	-	-	1,001	0,034
	hsp70l:klf2a_IRES_GFP	3	-	-	-	-	1,477	0,058
	hsp70l:kfl2b_IRES_GFP	3	-	-	-	-	1,9	0,14
Fig. 5D	wt	4	1,002	0,033	1,004	0,052	-	-
	*tnnt2a*MO	5	0,740	0,046	0,831	0,040	-	-
	ccm2	5	1,779	0,073	1,740	0,046	-	-
	ccm2 + *tnnt2a*MO	4	1,804	0,051	1,343	0,023	-	-

	Unpaired t-test (Fig.1A, 4A); 1-way ANOVA (Fig. 3E, 4A, 5D)	P value		
		klf2a	*klf2b*	*egfl7*
Fig. 1A	wt vs *ccm2*	**** P<0,0001	**** P<0,0001	-
Fig. 3E	wt vs *ccm2*	* P=0,0225	** P=0,0029	-
	wt vs wt + PTK787	n.s. P=0,994	n.s. P=0,993	-
	wt vs *ccm2* + PTK787	* P=0,0395	** P=0,0050	-
	ccm2 vs *ccm2* + PTK787	n.s. P=0,992	n.s. P=0,989	-
Fig. 4A	wt vs *ccm2*	-	-	** P=0,0098
Fig. 4A	ctrl vs *hsp70l:klf2a_IRES_GFP*	-	-	* P=0,017
	ctrl vs *hsp70l:klf2b_IRES_GFP*	-	-	*** P=0,0007
Fig.	wt vs *tnnt2a*MO	* P=0,0257	n.s. P=0,063	-

5D	wt vs *ccm2*	**** P<0,0001	**** P<0,0001	-
	wt vs *ccm2*;*tnnt2a*MO	**** P<0,0001	*** P=0,0006	-
	*tnnt2a*MO vs *ccm2*;*tnnt2a*MO	**** P<0,0001	**** P<0,0001	-
	ccm2 vs *ccm2*;*tnnt2a*MO	n.s. P=0,999	**** P<0,0001	-

mouse		n=	*Klf2*		Unpaired t-test
			Mean	SEM	Significant? P<0,05?
Fig 1B	control	5	1,009	0,0661	**
	iCCM2	5	1,690	0,1407	P=0,0023

HUVECs		n=	*KLF2*		*EGFL7*	
			Mean	SEM	Mean	SEM
Fig. 1C	Control	4	1	0	-	-
	siRNA-CCM2	4	16,93	4,247	-	-
Fig. 4B	Control siRNA	2	-	-	1	0,023
	siRNA-*ICAP1*	2	-	-	2,897	0,646
	siRNA-*KRIT1*	2	-	-	6,432	0,213
	siRNA-*CCM2*	2	-	-	5,428	0,249
Fig. 6A	Control siRNA	3	1,003	0,052	-	-
	siRNA-*ICAP1*	3	4,582	0,548	-	-
	siRNA-*KRIT1*	3	4,386	0,198	-	-
	siRNA-*CCM2*	3	5,291	0,053	-	-
	siRNA-*ITGB1*	3	1,002	0,041	-	-
	siRNA-*ICAP1* + siRNA-*ITGB1*	3	1,054	0,069	-	-
	siRNA-*KRIT1* + siRNA-*ITGB1*	3	0,914	0,221	-	-
	siRNA-*CCM2* + siRNA-*ITGB1*	3	1,393	0,103	-	-

	Paired t-test (Fig. 1C) and 1-way ANOVA test (Fig. 4B, 6A)	P value	
		KLF2	*EGFL7*
Fig. 1C	control vs siRNA-*CCM2*	* P=0,0331	-
Fig. 4B	control vs siRNA-*ICAP1*	-	* P=0,0467
	control vs siRNA-*KRIT1*	-	** P=0,0010
	control vs siRNA-*CCM2*	-	** P=0,0023
Fig. 6A	control vs siRNA-*ICAP1*	**** P<0,0001	-
	control vs siRNA-*KRIT1*	*** P=0,0001	-
	control vs siRNA-*CCM2*	**** P<0,0001	-
	siRNA-*ITGB1* vs siRNA-*ICAP1* + siRNA-*ITGB1*	n.s. P=0,982	-
	siRNA-*ITGB1* vs siRNA-*KRIT1* + siRNA-*ITGB1*	n.s. P=0,931	-
	siRNA-*ITGB1* vs siRNA-*CCM2* + siRNA-*ITGB1*	n.s. P=0,147	-

Heart extraction and microarray analyses. Entire hearts were extracted from wild-type and *ccm2*^{m201} mutant zebrafish embryos at 72 hpf by manual dissection as described elsewhere (Burns and MacRae, 2006). Total RNA was extracted with the RNeasy Micro Kit (Qiagen) according to the manufacturer's instructions. RNA quality was assessed on a 2100 Bioanalyzer RNA 6000 Nano chip (Agilent Technologies). RNA processing and chip hybridization was performed by imaGenes GmbH (Berlin, Germany) according to Agilent standard procedures. In brief, for each sample, 200ng of total RNA was subjected to a single amplification step and Cy3 labeling reaction. 1,5 µg of labeled cRNA were hybridized to Zebrafish (V2) Gene Expression Microarrays (G2519F-019161, 4x44K) and spot intensities recorded on a G2565BA scanner (Agilent Technologies). Microarrays were performed in single replicates for WT and *ccm2*^{m201} samples. Raw expression values were adjusted in R (www.r-project.org) using variance stability normalization (Huber et al., 2002). Enriched biological processes were identified by performing a functional annotation clustering analysis on DAVID (Huang et al., 2009). Only the most relevant terms were considered at significant p-values ($p<0.05$).

Selective plane illumination microscopy (SPIM) imaging. Timelapse data were recorded on a SPIM setup as described before (Huisken and Stainier, 2009). Transgenic zebrafish Tg(*kdrl:GFP*)^{s843} embryos were dechorionated at 24 hpf, anesthetized with Tricaine (200mg/L, Aldrich) and mounted in FEP fluorinated propylene ethylene (FEP) tubes filled with 3% methyl cellulose (Kaufmann et al., 2012). Between 33-53hpf, embryos were imaged every three minutes. Cell positions were tracked manually based on maximal intensity projections using the Wand and the Flood Fill Tool in Fiji (Schindelin et al., 2012). The ratio of proliferative vs. non-proliferative endocardial cells was determined based on these recordings and is shown as mean with SEM. Each dividing cell and its daughter cell were assigned a unique color to visualize mitotic events. The statistical analysis was performed in Prism 5 (GraphPad) as an unpaired t-test. Means are statistically significantly different if $P < 0.05$.

embryo	Number of (tracked) cells undergoing mitosis	Total number of (tracked) cells	Mean ratio +/- SEM	Unpaired t-test P value
*tnnt2a*MO #1	0	30	0,104 +/- 0,104	* P=0,034
*tnnt2a*MO #2	5	24		
ccm2;*tnnt2a*MO #1	30	33	0,821 +/- 0,087	
ccm2;*tnnt2a*MO #2	33	45		

Video angiography during neurosurgical procedures. 25 mg of indocyanine green (ICG) was injected intravenously before surgical removal. The surgical situs was illuminated by a near-infrared laser excitation light source (lambda = 780 nm). The intravascular fluorescence of ICG (maximal lambda = 835 nm) was then recorded by a non-intensified video camera, with optical filtering to block ambient and laser light for collection of only ICG-induced fluorescence (Raabe et al., 2003).

REFERENCES

Ablooglu,A.J., Tkachenko,E., Kang,J., and Shattil,S.J. (2010). Integrin alphaV is necessary for gastrulation movements that regulate vertebrate body asymmetry. Development *137*, 3449-3458.

Boulday,G., Blecon,A., Petit,N., Chareyre,F., Garcia,L.A., Niwa-Kawakita,M., Giovannini,M., and Tournier-Lasserve,E. (2009). Tissue-specific conditional CCM2 knockout mice establish the essential role of endothelial CCM2 in angiogenesis: implications for human cerebral cavernous malformations. Dis. Model. Mech. *2*, 168-177.

Burns,C.G. and MacRae,C.A. (2006). Purification of hearts from zebrafish embryos. Biotechniques *40*, 274-278.

Bustin,S.A., Benes,V., Garson,J.A., Hellemans,J., Huggett,J., Kubista,M., Mueller,R., Nolan,T., Pfaffl,M.W., Shipley,G.L., Vandesompele,J., and Wittwer,C.T. (2009). The MIQE guidelines: minimum information for publication of quantitative real-time PCR experiments. Clin. Chem. *55*, 611-622.

Chan,J., Bayliss,P.E., Wood,J.M., and Roberts,T.M. (2002). Dissection of angiogenic signaling in zebrafish using a chemical genetic approach. Cancer Cell *1*, 257-267.

Faurobert,E., Rome,C., Lisowska,J., Manet-Dupe,S., Boulday,G., Malbouyres,M., Balland,M., Bouin,A.P., Keramidas,M., Bouvard,D., Coll,J.L., Ruggiero,F., Tournier-Lasserve,E., and Albiges-Rizo,C. (2013). CCM1-ICAP-1 complex controls beta1 integrin-dependent endothelial contractility and fibronectin remodeling. J. Cell Biol. *202*, 545-561.

Herwig,L., Blum,Y., Krudewig,A., Ellertsdottir,E., Lenard,A., Belting,H.G., and Affolter,M. (2011). Distinct cellular mechanisms of blood vessel fusion in the zebrafish embryo. Curr. Biol. *21*, 1942-1948.

Huang,C.J., Tu,C.T., Hsiao,C.D., Hsieh,F.J., and Tsai,H.J. (2003). Germ-line transmission of a myocardium-specific GFP transgene reveals critical regulatory elements in the cardiac myosin light chain 2 promoter of zebrafish. Dev. Dyn. *228*, 30-40.

Huang,d.W., Sherman,B.T., and Lempicki,R.A. (2009). Systematic and integrative analysis of large gene lists using DAVID bioinformatics resources. Nat. Protoc. *4*, 44-57.

Huber,W., von,H.A., Sultmann,H., Poustka,A., and Vingron,M. (2002). Variance stabilization applied to microarray data calibration and to the quantification of differential expression. Bioinformatics. *18 Suppl 1*, S96-104.

Huisken,J. and Stainier,D.Y. (2009). Selective plane illumination microscopy techniques in developmental biology. Development *136*, 1963-1975.

Jin,S.W., Beis,D., Mitchell,T., Chen,J.N., and Stainier,D.Y. (2005). Cellular and molecular analyses of vascular tube and lumen formation in zebrafish. Development *132*, 5199-5209.

Jowett,T. and Lettice,L. (1994). Whole-mount in situ hybridizations on zebrafish embryos using a mixture of digoxigenin- and fluorescein-labelled probes. Trends Genet. *10*, 73-74.

Kaufmann,A., Mickoleit,M., Weber,M., and Huisken,J. (2012). Multilayer mounting enables long-term imaging of zebrafish development in a light sheet microscope. Development *139*, 3242-3247.

Kwan,K.M., Fujimoto,E., Grabher,C., Mangum,B.D., Hardy,M.E., Campbell,D.S., Parant,J.M., Yost,H.J., Kanki,J.P., and Chien,C.B. (2007). The Tol2kit: a multisite gateway-based construction kit for Tol2 transposon transgenesis constructs. Dev. Dyn. *236*, 3088-3099.

Livak,K.J. and Schmittgen,T.D. (2001). Analysis of relative gene expression data using real-time quantitative PCR and the 2(-Delta Delta C(T)) Method. Methods *25*, 402-408.

Mably,J.D., Chuang,L.P., Serluca,F.C., Mohideen,M.A., Chen,J.N., and Fishman,M.C. (2006). santa and valentine pattern concentric growth of cardiac myocardium in the zebrafish. Development *133*, 3139-3146.

Mably,J.D., Mohideen,M.A., Burns,C.G., Chen,J.N., and Fishman,M.C. (2003). heart of glass regulates the concentric growth of the heart in zebrafish. Curr. Biol. *13*, 2138-2147.

Nicoli,S., Standley,C., Walker,P., Hurlstone,A., Fogarty,K.E., and Lawson,N.D. (2010). MicroRNA-mediated integration of haemodynamics and Vegf signalling during angiogenesis. Nature *464*, 1196-1200.

Raabe,A., Beck,J., Gerlach,R., Zimmermann,M., and Seifert,V. (2003). Near-infrared indocyanine green video angiography: a new method for intraoperative assessment of vascular flow. Neurosurgery *52*, 132-139.

Sehnert,A.J., Huq,A., Weinstein,B.M., Walker,C., Fishman,M., and Stainier,D.Y. (2002). Cardiac troponin T is essential in sarcomere assembly and cardiac contractility. Nat. Genet. *31*, 106-110.

Schindelin,J., Arganda-Carreras,I., Frise,E., Kaynig,V., Longair,M., Pietzsch,T., Preibisch,S., Rueden,C., Saalfeld,S., Schmid,B., Tinevez,J.Y., White,D.J., Hartenstein,V., Eliceiri,K., Tomancak,P., and Cardona,A. (2012). Fiji: an open-source platform for biological-image analysis. Nat. Methods *9*, 676-682.

Veerkamp, J., Rudolph, F., Cseresnyes, Z., Priller, F., Otten, C., Renz, M., Schaefer, L., and Abdelilah-Seyfried, S. (2013). Unilateral dampening of Bmp activity by nodal generates cardiac left-right asymmetry. Dev Cell. *24*, 660-667.

Vermot,J., Forouhar,A.S., Liebling,M., Wu,D., Plummer,D., Gharib,M., and Fraser,S.E. (2009). Reversing blood flows act through klf2a to ensure normal valvulogenesis in the developing heart. PLoS. Biol. *7*, e1000246.

Villefranc,J.A., Amigo,J., and Lawson,N.D. (2007). Gateway compatible vectors for analysis of gene function in the zebrafish. Dev. Dyn. *236*, 3077-3087.

Westerfield,M., Doerry,E., Kirkpatrick,A.E., Driever,W., and Douglas,S.A. (1997). An on-line database for zebrafish development and genetics research. Semin. Cell Dev. Biol. *8*, 477-488.

Supplemental Movies and Spreadsheets

Click here to download Supplemental Movies & Spreadsheets: Renz_Supplementary movie 1.mov

Supplemental Movies and Spreadsheets

Click here to download Supplemental Movies & Spreadsheets: Renz_Supplementary movie 2.mov

Supplemental Movies and Spreadsheets

Click here to download Supplemental Movies & Spreadsheets: Renz_Supplementary_movie 3.mp4